EXPLORING FREE FLOATING PLANETS WITH MICROLENSING

A DISSERTATION SUBMITTED TO THE UNIVERSITY OF MANCHESTER

FOR THE DEGREE OF MASTER OF SCIENCE BY RESEARCH

IN THE FACULTY OF ENGINEERING AND PHYSICAL SCIENCES

2012

By

Vasiliki Fragkou

School of Physics and Astronomy

Jodrell Bank Centre for Astrophysics

Contents

3 Microlensing Light Curves Modelling   50

4 Planetary Events: Free Floating or Bound Planets?   63

5 Conclusions and Future Work   78

References   80

Word count: 14133

List of Tables

List of Figures

Abstract

About one year ago, the MOA microlensing team announced the discovery of a free floating planet population with the method of gravitational microlensing (Sumi et al. 2011). In this thesis, we test the possibility of these planets being in reality bound but getting confused as free floating because of the shape of their light curve.

Following a review of extrasolar planets and a description of the method of gravitational microlensing, we simulate binary lensing events produced by several combinations of parameters for the source star, the lens star and the planet, the light curves of which, afterwards, are fitted to the light curve of a single lensing event. After rejecting some of the simulated events because of their unclear light curve, we determine which of the simulated binary microlensing events produce a light curve that cannot be differentiated to that of a free floating planet, their fitting parameters, the parameters that produced them and their relative frequency. Our results indicate that, for Jupiter mass free-floating planets, we expect less than 0.1 out of the 1000 events analysed by MOA to look like free floating systems yet be caused by bound planets within 100 AU of their host star.

As a result, the comparison of our results with the results of Sumi et al. (2011) reveals that the population of exoplanets that Sumi et al. (2011) detected consists either from actually unbound planets or from bound planets with sky-projected separations from their host, longer than 100 AU.

University of Manchester
Vasiliki Fragkou
Master of Science by Research (MSc)
Exploring Free Floating Planets with Microlensing
29 August 2012

Declaration

No portion of the work referred to in this thesis has been submitted in support of an application for another degree or qualification of this or any other university or other institute of learning.

Vasiliki Fragkou

University of Manchester

Jodrell Bank Centre for Astrophysics

Alan Turing Building

Oxford Road

Manchester

M13 9PL

U.K.

Copyright

(i) The author of this thesis (including any appendices and/or schedules to this thesis) owns certain copyright or related rights in it (the "Copyright"), and she has given The University of Manchester certain rights to use such Copyright, including for administrative purposes.

(ii) Copies of this thesis, either in full or in extracts and whether in hard or electronic copy, may be made **only** in accordance with the Copyright, Designs and Patents Act 1988 (as amended) and regulations issued under it or, where appropriate, in accordance with licensing agreements which the University has from time to time. This page must form part of any such copies made.

(iii) The ownership of certain Copyright, patents, designs, trade marks and other intellectual property (the "Intellectual Property") and any reproductions of copyright works in the thesis, for example graphs and tables ("Reproductions"), which may be described in this thesis, may not be owned by the author and may be owned by third parties. Such Intellectual Property and Reproductions cannot and must not be made available for use without the prior written permission of the owner(s) of the relevant Intellectual Property and/or Reproductions.

(iv) Further information on the conditions under which disclosure, publication and commercialisation of this thesis, the Copyright and any Intellectual Property and/or Reproductions described in it may take place is available in the University IP Policy (see http://www.campus.manchester.ac.uk/medialibrary/policies/intellectualproperty.pdf), in any relevant Thesis restriction declarations deposited in the University Library, The University Library's regulations (see http://www.manchester.ac.uk/library/aboutus/regulations) and in The University's policy on presentation of Theses.

Acknowledgements

The Author

The author was born in Athens, Greece and in 2007 she attended, with the Erasmus program, the University of La Laguna, Spain where she mostly attended courses on observational astronomy. In 2011, she obtained an undergraduate degree in Physics at the Aristotle University of Thessaloniki, with a specialization in Astronomy, where she concluded her undergraduate dissertation about the Antikythera Mechanism. In September 2011, she came to Manchester, UK to attend an MSc programme at the University of Manchester, Jodrell Bank Centre for Astrophysics and the results of these studies are presented in this thesis.

Vasiliki Fragkou

Jodrell Bank Centre for Astrophysics,

Alan Turing Building,

University of Manchester,

Oxford Road,

Manchester,

M13 9PL.

Supervisor: **Eamonn Kerins**

Advisor: **Clive Dickinson**

*Dedicated to all the people who never
stop searching for the truth.*

.

….οὐδέν τό ἐμποδοστατῆσον ἐστι πρός τήν ἀπειρίαν τῶν κόσμων.
(….there will be nothing to hinder an infinity of worlds.)

~ Epicurus ~

We are just an advanced breed of monkeys on a minor
planet of a very average star. But we can understand the
Universe. That makes us something very special.

~ Stephen Hawking ~

CHAPTER 1

INTRODUCTION TO EXTRASOLAR PLANETS

1.1 Historical References

For thousands of years, humans doubted about the unique existence of our world. Ancient Greek philosophers such as Democritus[1] (Kirk et al. 1962, p418) and Epicurus[2] supported the view that our world is not the only one in the Universe. Epicurus, in one of his letters to Herodotus mentions that: "There is an infinite number of worlds in the Universe, both like and unlike this world of ours."[3] . On the contrary, the ancient Greek philosopher Aristotle[4], whose ideas were meant to influence the philosophical views for the following centuries, was convinced that our world is unique (Kirk et al. 1962, p127). As a consequence, the idea of the existence of other worlds did not develop until the end of 17th century, after Copernicus published his theory about Heliocentrism (Copernicus 1543) and Galileo proved it with his observations (Galilei 1989), when the astronomer Christiaan Huygens published his work "Cosmotheoros (1698)" (Huygens et al. 1989). Humanity was now ready to accept this idea and a lot of astronomers were trying to prove it for the following centuries, something that only happened at the end of 20th century with the detection of the first extrasolar planets.

The accidental discovery of three planets, with masses of approximately 2.8, 3.4 and 0.015 $M_{\oplus}$ and periods of 98.22, 66.54 and 25.34 days respectively, orbiting the millisecond pulsar PSR1257+12, (Wolszczan et al. 1992; Wolszczan 1994) demonstrated the existence of exoplanetary systems. Furthermore, a few years later, Mayor et al. (1995), detected a giant planet orbiting the solar type star 51 Pegasi with a semi-major axis of 0.05 AU. This discovery was the first detection of an exoplanet in an orbit around a star, which, the following year, led to the discovery of more exoplanets orbiting the stars 70 Virginis (Marcy et al. 1996) and 47 Ursae Majoris (Butler et al. 1996) and few years later, to the detection of the first multiple exoplanetary system around the star Upsilon Andromedae (Lissauer 1999). Actually, the first exoplanet ever detected was a planet orbiting the star

---

[1] (Democretus, 460-370 B.C.).
[2] (Epicurus, 341-270 B.C).
[3] (Epicurus, letter to Herodotus, 3th century B.C., paragraph: 15).
[4] (Aristotle, 384-322 B.C.).

Gamma Cephei (Campbell et al. 1988), but it only was confirmed to be a planetary object in 2003 (Hatzes et al. 2003).

To date more than 750 extrasolar planets have been detected, with one of them in an orbit around a binary star (Doyle et al. 2011), in 620 planetary systems and from those systems, 102 are multiplanetary ones (Figure 1.1) (Schneider 2012).
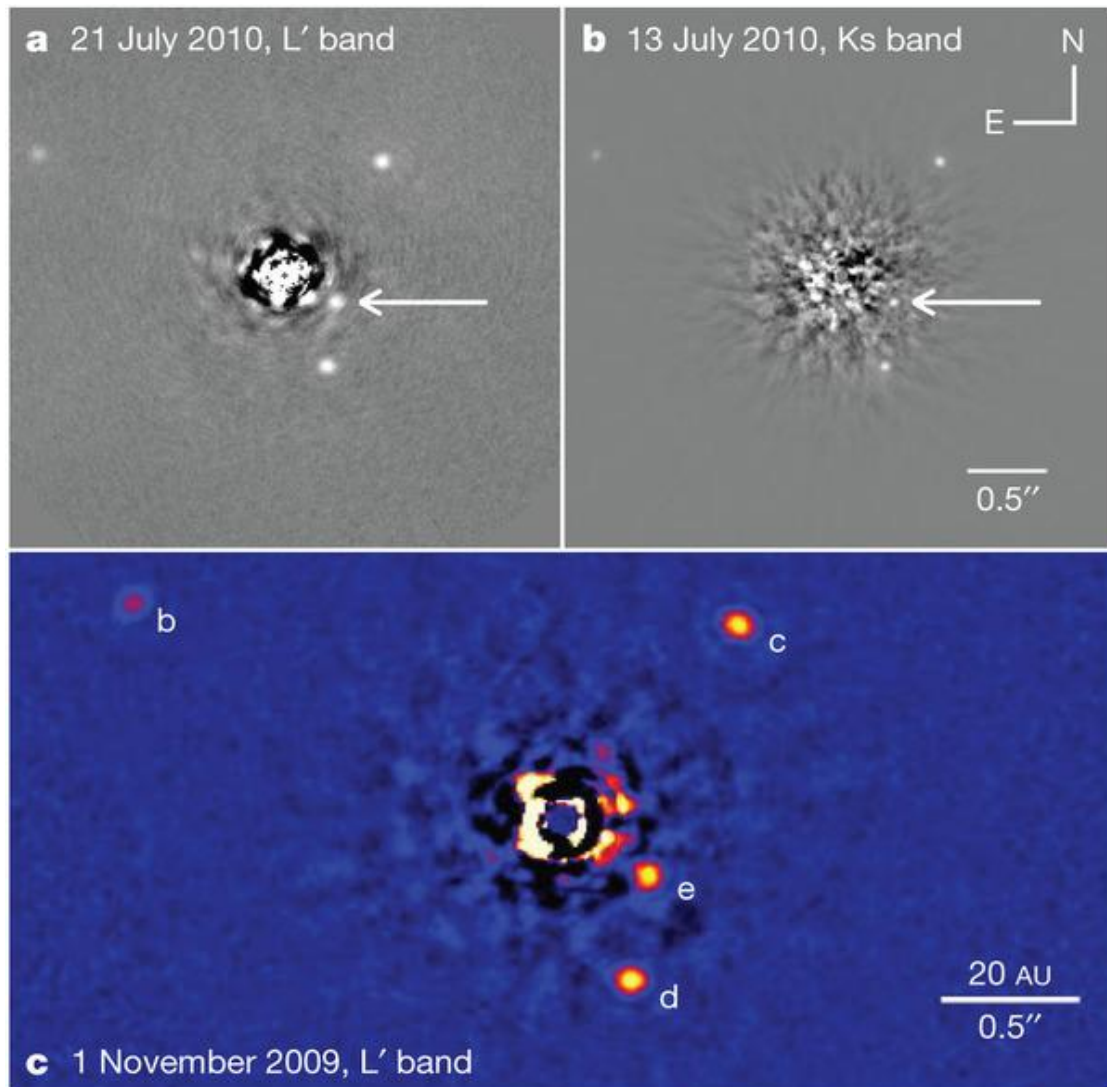
Figure 1.1 Near-infrared observations of the multiplanetary system around the star HR 8799. The arrow in the images a and b indicates the position of the planet HR 8799e. [Figure Credit: Adapted by permission from Macmillan Publishers Ltd: [NATURE] (Marois et al. 2010; p1080), copyright (2010)]

1.2 Statistical Analysis of Extrasolar Planets

The following is a statistical analysis of extrasolar planets. The data for this analysis came from Schneider (2012).

In Figure 1.2a, we can see a planet mass vs planet semi-major axis correlation diagram where the different methods of detection are noticeable. It is obvious that the majority of the detected exoplanets have a mass from 0.01 to 10 M_{Jup} and a semi-major axis from 0.01 to 10 AU. In Figure 1.2b, we see a planet mass vs planet period correlation diagram and it can be seen that most of the detected exoplanets have a period from 0.1 to 5000 days, but there are many with much bigger periods, with one among them with a period of more than 700000 days (1918 years). In addition, most of the exoplanets have been detected with the radial-velocity and astrometry techniques. To specify, the majority of the extrasolar planets that have already been detected (mainly from ground based observations) have a mass bigger than the mass of Jupiter (416 planets) and only 5 exoplanets have a mass comparable with that of Earth or smaller (Figure 1.3) (The Kepler mission, which searches for low mass exoplanets with the transit method has announced the detection of more than 2000 planetary candidates, which have not yet been confirmed (Batalha et al. 2012)). Moreover, among all the detected exoplanets there are 206 "hot Jupiters" and 17 "hot Neptunes" (the definitions "Hot Jupiters" and "hot Neptunes" are used for planets with periods smaller than 14 days and masses bigger than 0.2 M_{Jup} and from 10 to 20 $M_{\oplus}$ respectively (Sato et al. 2005)).

a.Planet Mass-Planet Semi-Major Axis

Radial-velocity/Astrometry
Transits
Microlensing
Imaging
Timing

Planet Sem. Maj. Axis (α/AU)

Planet Mass (Mp/MJup)

b.Planet Mass-Planet Period

Radial-velocity/Astrometry
Transits
Microlensing
Imaging
Timing

Planet Period (P/days)

Planet Mass (Mp/MJup)
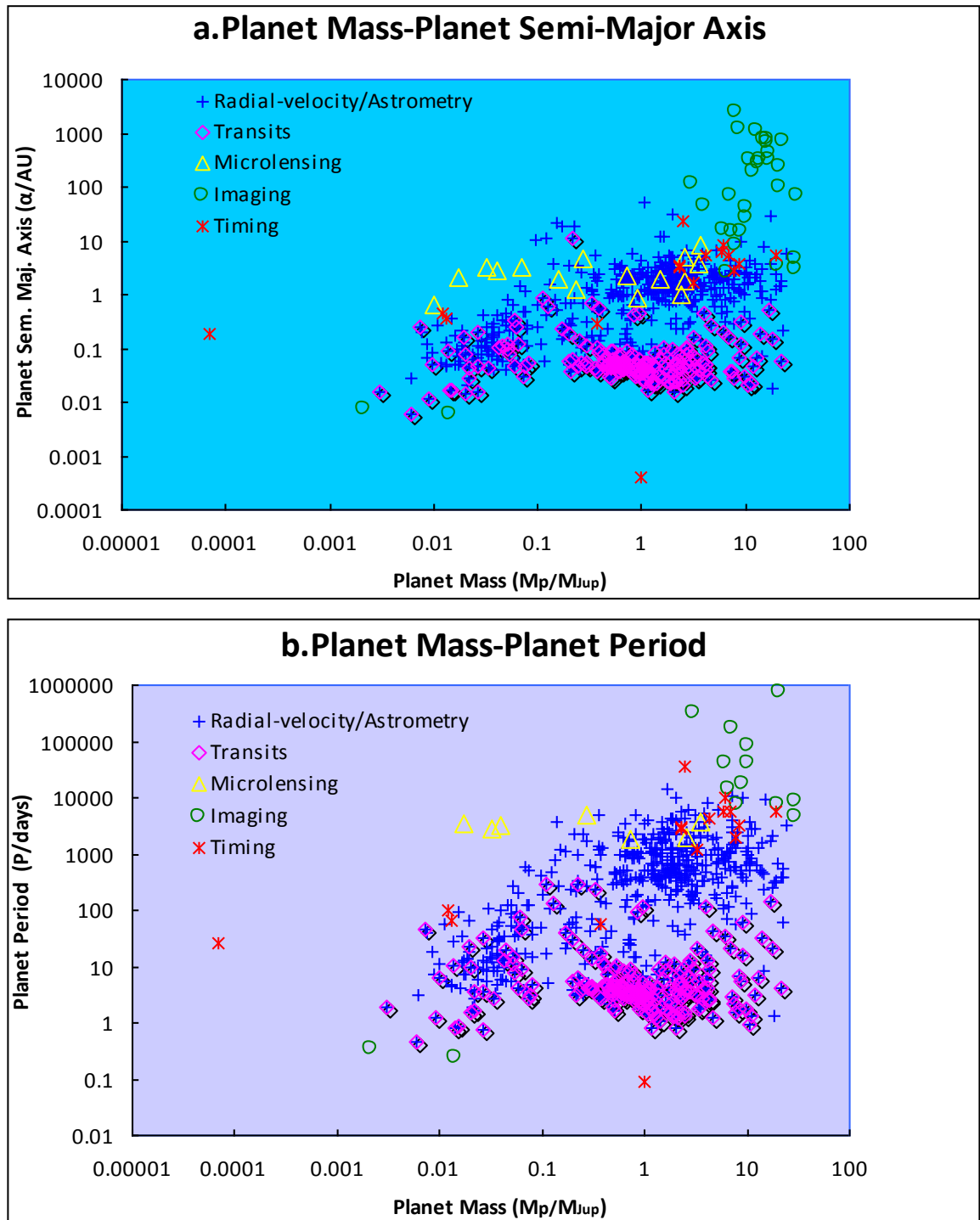
Figure 1.2   Planet mass-planet semi-major axis (**a**) and planet mass-planet period (**b**) correlation diagrams in logarithmic axes. We can distinguish different methods of detection considering data points with colour blue for radial-velocity and astrometry, pink for transits, yellow for microlensing, green for direct imaging and red for timing method. The exoplanets that have been detected with transits have also been detected with the radial-velocity technique as these two techniques compared, provide accurate results for the mass of the planets (Udru et al. 2007). The data for this diagram have been provided from Schneider (2012).
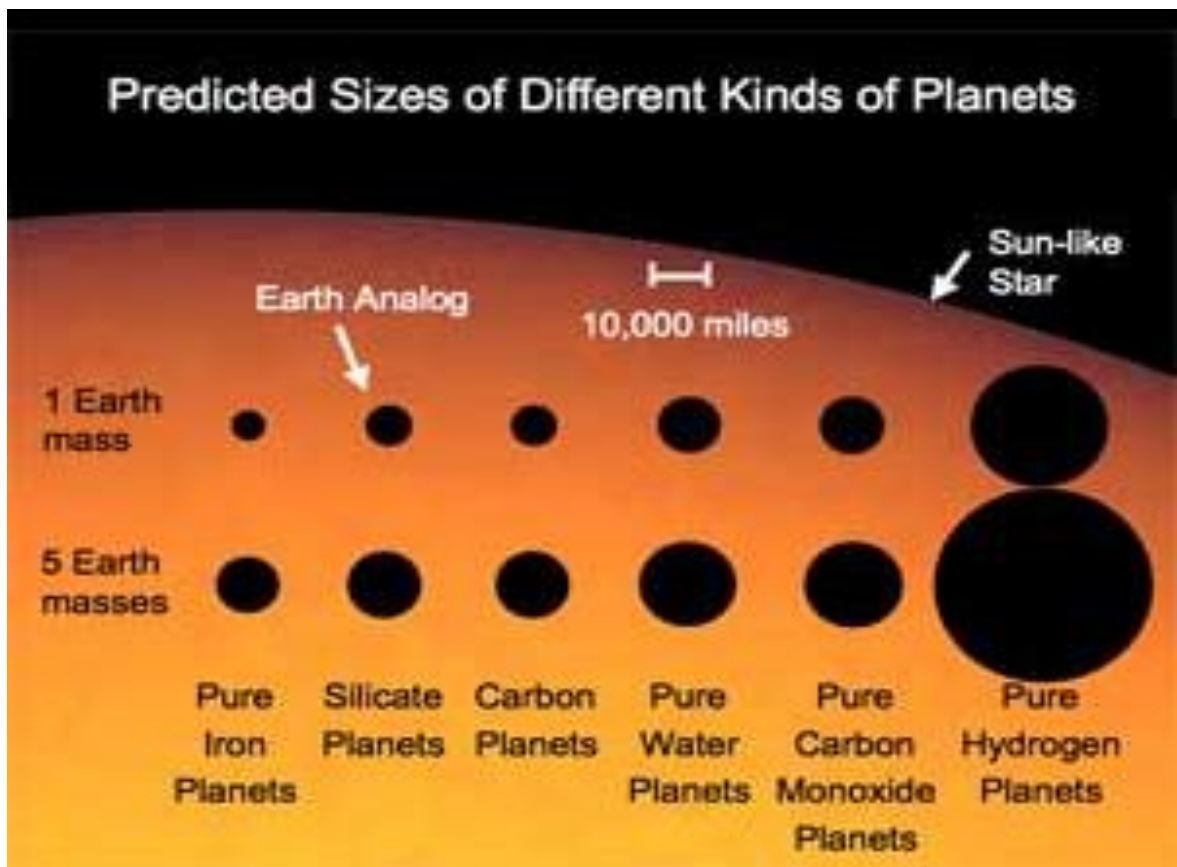
Figure 1.3 Predicted sizes of planets of different composition. [Figure Credit: Marc Kuchner/NASA GSFC, http://www.nasa.gov/centers/goddard/news/topstory/2007/earthsized_planets.html, date of access: 16th of July 2012]

Furthermore, 528 planets have an eccentricity from 0.00002 to 0.8 (Figure 1.4), with the eccentricity of single planets being typically larger than that of planets in multiplanetary systems (Wright et al. 2009). Moreover, in Figure 1.5 we can see that the radius of the detected exoplanets, ranges from 0.05 to 2.18 R_{Jup} with most of them having a radius around 1.1 R_{Jup}, but the sample is still modest, since only the radius of 251 exoplanets have already been measured and most of them have been detected with astrometry or the radial-velocity technique.
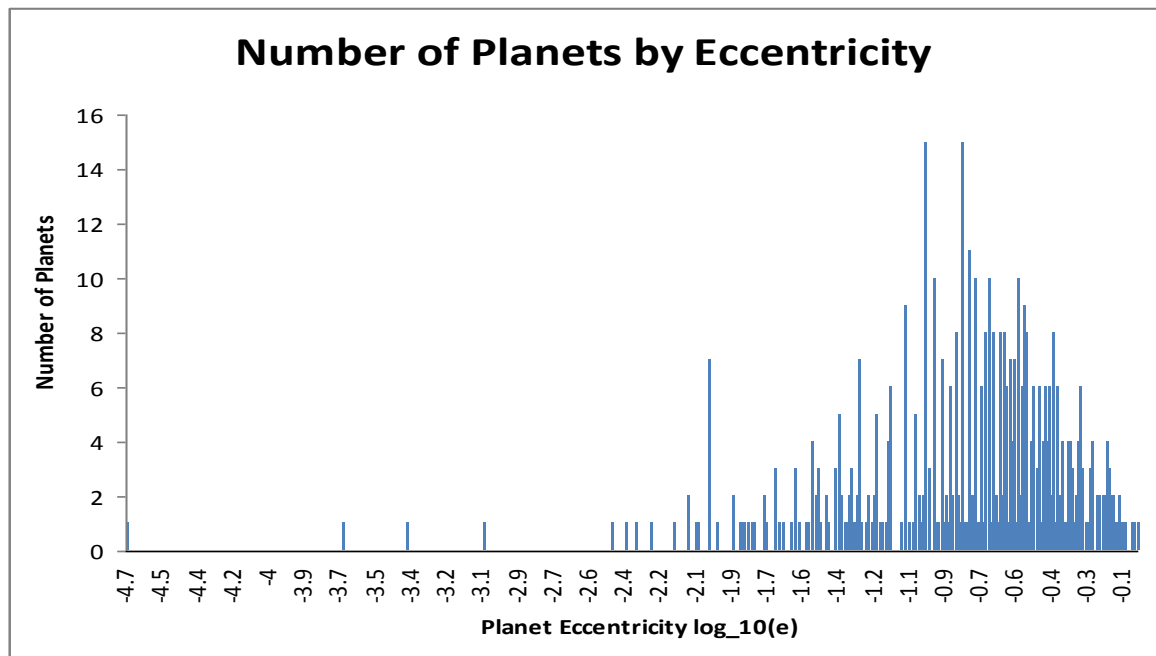
Figure 1.4 Histogram of the eccentricity of the detected exoplanets. The data for this diagram have been provided from Schneider (2012).
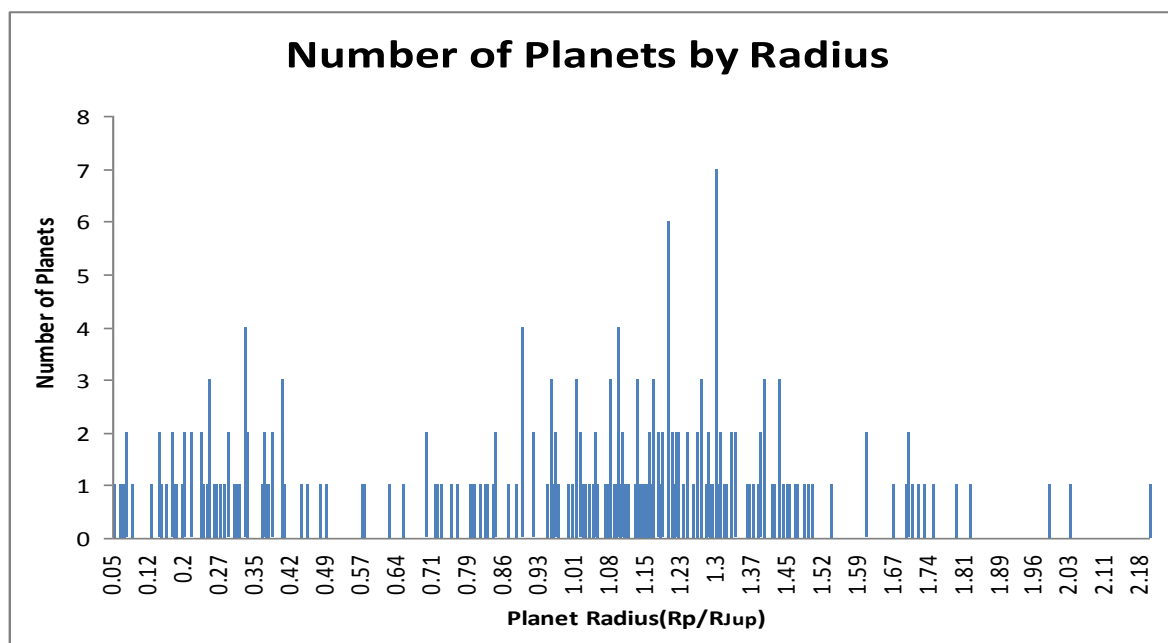
Figure 1.5 Histogram of the radius of the detected exoplanets, the radius of which it has already been measured (251 exoplanets). The data for this diagram have been provided from Schneider (2012).

In addition, the orbit of exoplanets that have a short period (P<20 days) approximates a circular orbit (Laughlin 2000). Moreover, if one planet is already detected orbiting a star, the possibility of finding a second planet orbiting the same star, increases by 7% of the possibility of detecting the first planet (Udry et al. 2007).

Considering the stars, the majority of solar-like stars host at least one planet and 14% of them have a planet with a mass bigger than 50 $M_\oplus$ (Mayor et al. 2011). The metallicity [Fe/H] of almost all the stars that have a planetary companion ranges from -1.0 to +0.6, however there is one star that has a metallicity smaller than -2.0 (Figure 1.6). Furthermore as it can be seen in Figures 1.7 and 1.8, the majority of the stars that host detected exoplanets have a mass comparable to the mass of the Sun and a radius from 0.5 to 5 R_{sun}

Concluding, Cassan et al. (2012), indicates that, statistically, all the stars in our galaxy are hosts to one or more planets. This result is based on the microlensing technique.
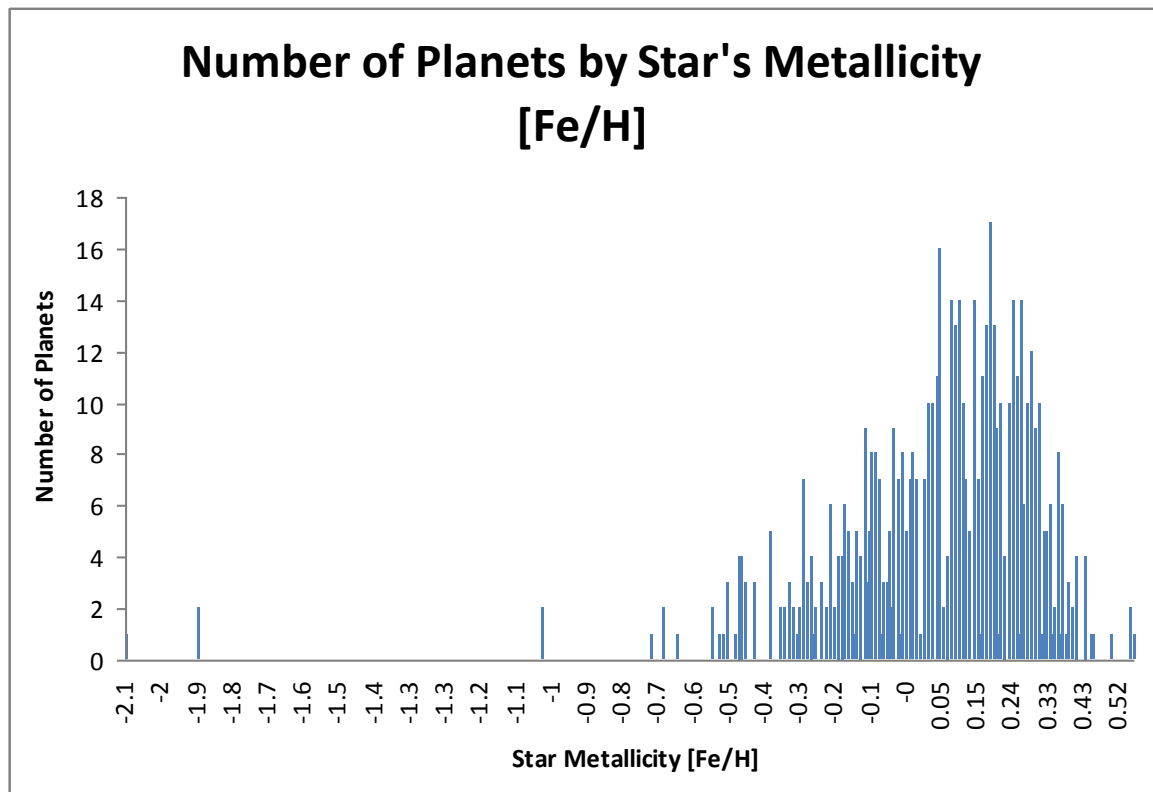
Figure 1.6   Histogram of the metallicity [Fe/H] of the stars that host the detected exoplanets. The data for this diagram have been provided from Schneider (2012).
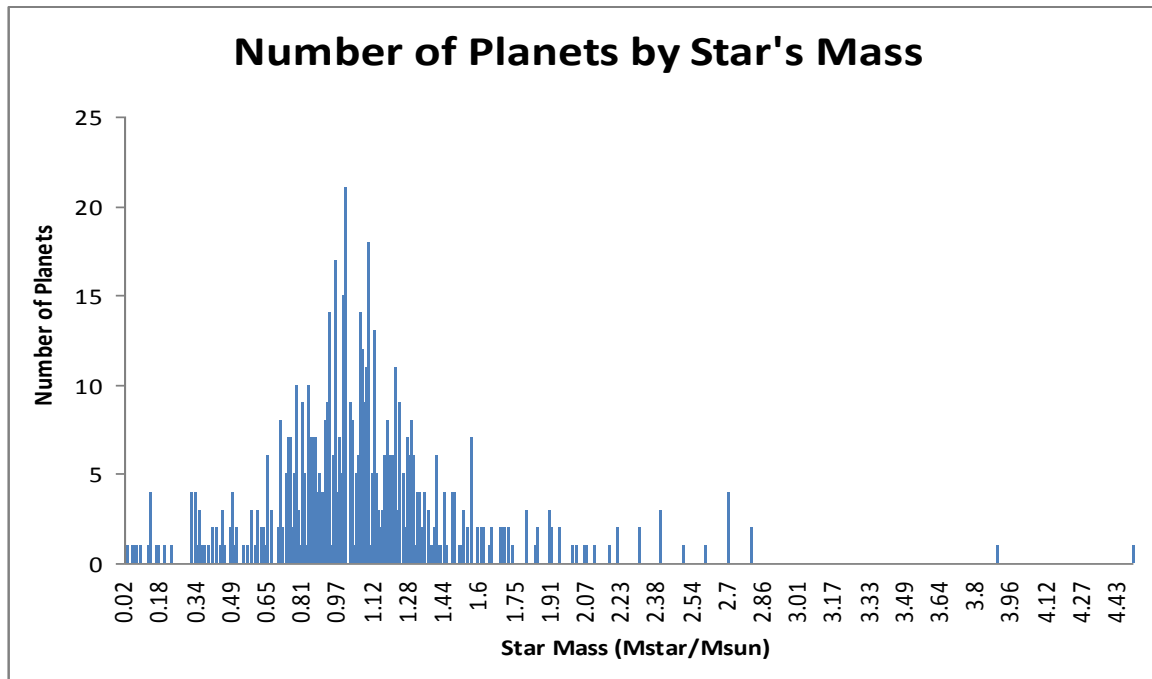
Figure 1.7   Histogram of the mass (M_{sun}) of the stars that host the detected exoplanets. The data for this diagram have been provided from Schneider (2012).
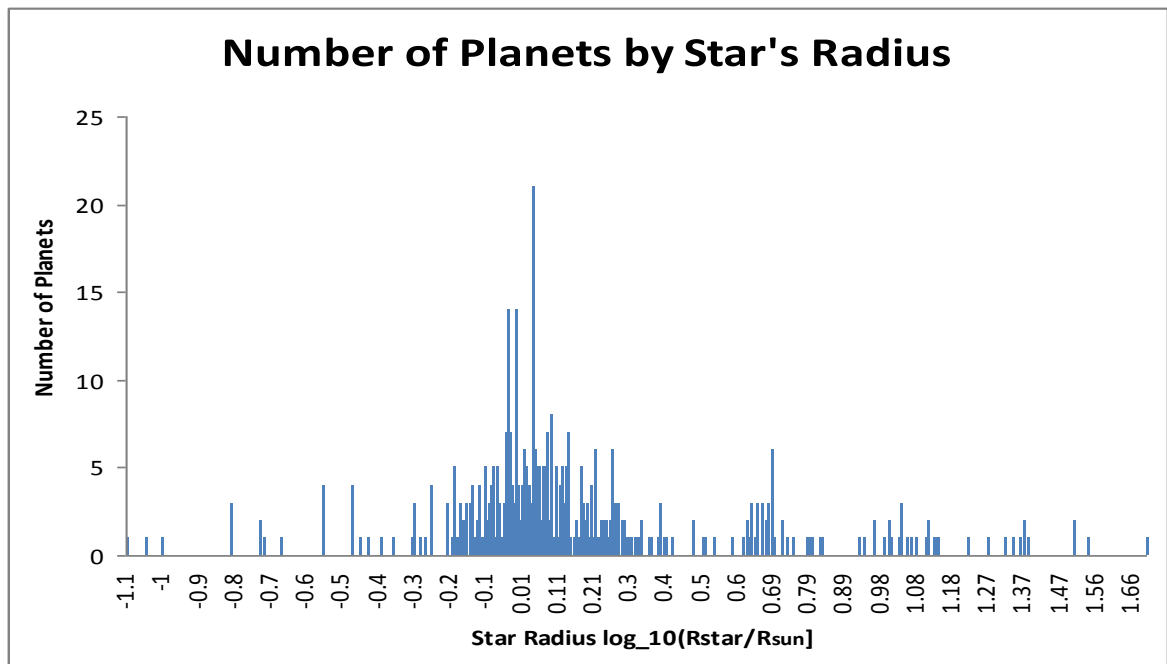
Figure 1.8   Histogram of the radius (R_{sun}) of the stars that host the detected exoplanets. The data for this diagram have been provided from Schneider (2012).

1.3 Habitable Planets

One very important property of an extrasolar planet is its habitability. A planet can be considered as a habitable one when it lies in the habitable zone, which is determined from the planet-host star distance, which should be appropriate for the existence of liquid water on the planet's surface (Kasting et al. 1993; Gehman et al. 1996). Another factor that should be taken into account for the habitability of a planet is its stability; a planet has to be stable in the habitable zone for a time range enough for the development of life (Jones et al. 2001). Therefore, if we suppose that extraterrestrial life exists and is similar to the life on Earth (liquid water is required for carbon-based life (Owen 1980)), these habitable planets should be the first target for searching for it (Perryman 2000) or a target for a possible future colonization by humans. Even for a free floating planet it might be possible to have the appropriate temperature for the presence of liquid water on its surface, as the internal heating of the planet could be enough for allowing water to remain in its liquid state (Stevenson 1999). In addition, despite the fact that the available data indicate that massive planets are more common (Schneider 2012), Ida et al. (2004) indicates that the habitable planets are as numerous as the detectable gas giants, or even more abundant.

To date, it is believed that five of the 777 confirmed detected exoplanets (Figure 1.9) and 27 of the 2321 planetary candidates detected by the Kepler mission (the majority of them are as yet unconfirmed exoplanets) might be considered as habitable ones (Méndez et al. 2012).
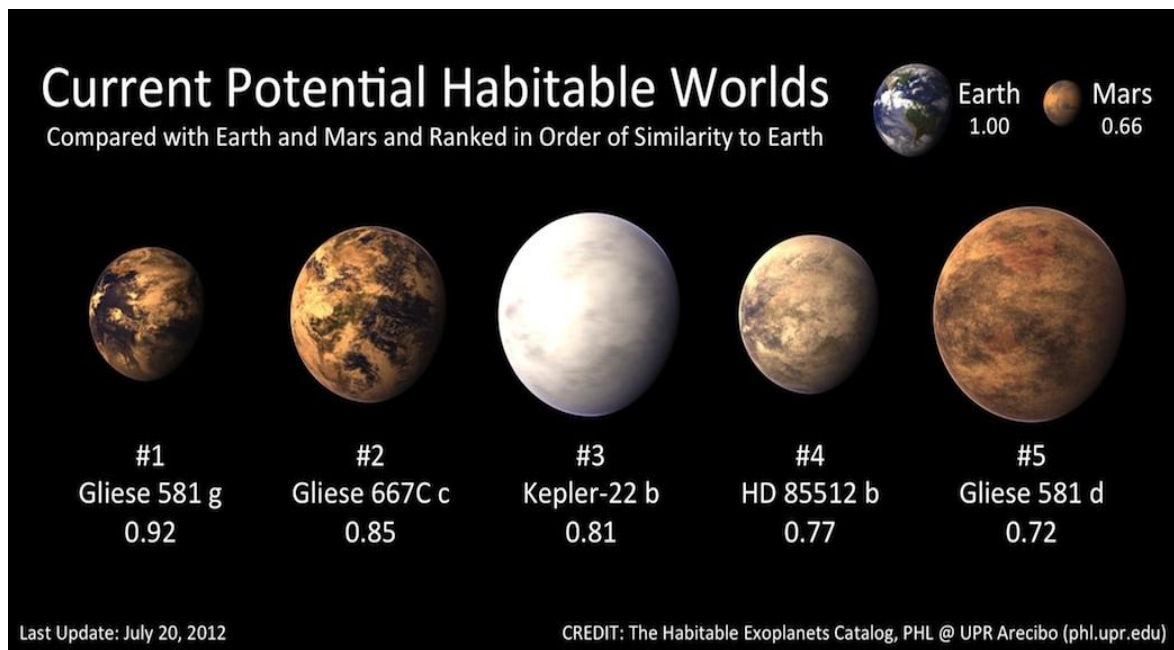
Figure 1.9 The five detected exoplanets that are considered to be habitable ones, compared with Earth and Mars using ESI (Earth Similarity Index). Planets with ESI larger than 0.8 can be considered to be very similar to the Earth and as a consequence to host life, but planets with ESI from 0.7 to 0.8 can still host microbial life. [Figure Credit: Méndez et al. 2012, The Habitable Exoplanet Catalog, Planetary Habitability Laboratory@ UPR Arecibo (http://phl.upr.edu); http://phl.upr.edu/projects/habitable-exoplanets-catalog/, date of access: 20th of August 2012].

1.4 Free Floating Planets

Although the planets are usually in an orbit around a star, there is one special category of exoplanets that are not bound to any host (Zapatero et al. 2000). The planets of this kind are named free floating planets and they first got the attention of the scientific community when Zapatero et al. (2000) discovered a population of free floating planet candidates in the σ Orionis star cluster with the method of direct imaging. This discovery was followed by the detection of some more free floating planet candidates in Taurus (Quanz et al. 2010), the discovery of a population of planet-like objects that do not seem to be bound to any host with the method of gravitational microlensing (Figures 1.10, 1.11) (Sumi et al. 2011) and finally with the detection of 23 new planetary mass objects in the σ Orionis cluster (Peňa et al. 2012).
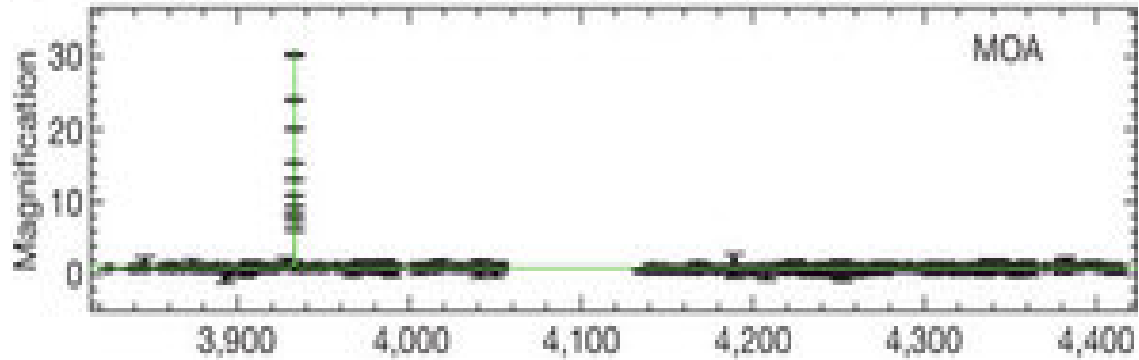
Figure 1.10 The light curve of a free floating planet candidate (microlensing event MOA-ip-10). [Figure Credit: Adapted by permission from Macmillan Publishers Ltd: [NATURE] (Sumi et al. 2011; p350), copyright (2011)]
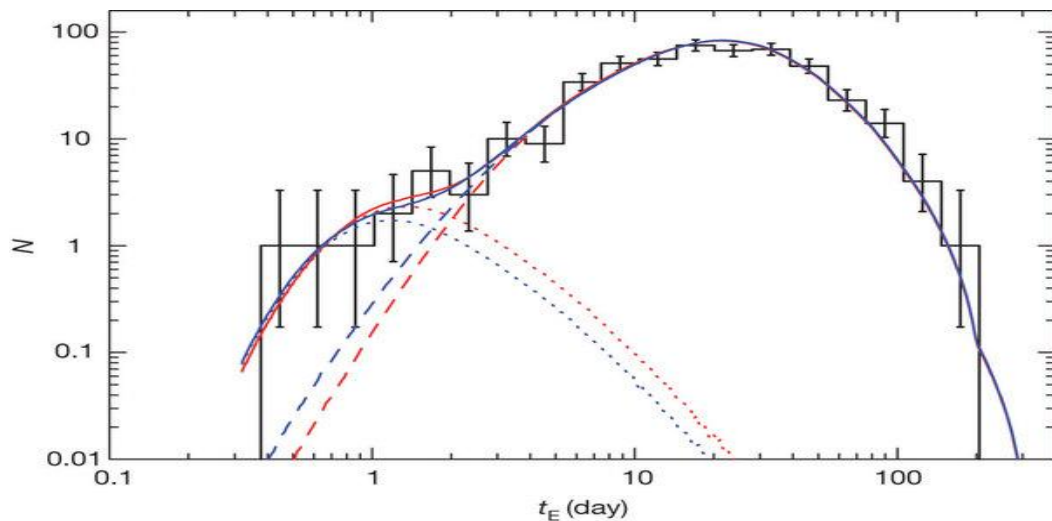
Figure 1.11 Histogram of the Einstein timescale t_E (defines how long a microlensing event lasts and depends on the mass of the lensing object (see section 2.1, Equation 2.15)) of 474 microlensing events analysed by Sumi et al. (2011) and their error bars. The red lines indicate the best-fit models with the power law mass function and the blue lines indicate the best-fit models with the log-normal mass function. Moreover, the dotted lines indicate the planetary mass population, the dashed lines represent models for brown dwarf, stellar remnant and stellar populations and the solid lines are their sums. [Figure Credit: Adapted by permission from Macmillan Publishers Ltd: [NATURE] (Sumi et al. 2011; p350), copyright (2011)]

Furthermore, Strigari et al. 2012 indicates that the planetary objects with masses between 10^{-8} and 10^{-2} $M_\odot$ that are not bound to any host may be a hundred thousand times more common than the stars in the main sequence.

1.5 Methods of Detecting Extrasolar Planets

There are various methods that are used for the detection of extrasolar planets. These methods are the radial-velocity technique, astrometry, the transit method, gravitational microlensing, direct imaging and pulsar timing. Consequently, we give a brief description of each one of these methods and we discuss their advantages and disadvantages.

1.5.1 Radial Velocity Technique

The radial-velocity technique is the most common method used for the detection of exoplanets and this was the method that has been used for the discovery of 51 Peg b the first exoplanet detected orbiting a star (Mayor et al. 1995).

This technique is actually based on the detection of the periodic motion of a star (using the Doppler Effect) around its system's barycentre due to gravitational effects caused by the orbital motion of a planet around it (Figure 1.12) (Marcy et al. 1998; Perryman 2000).
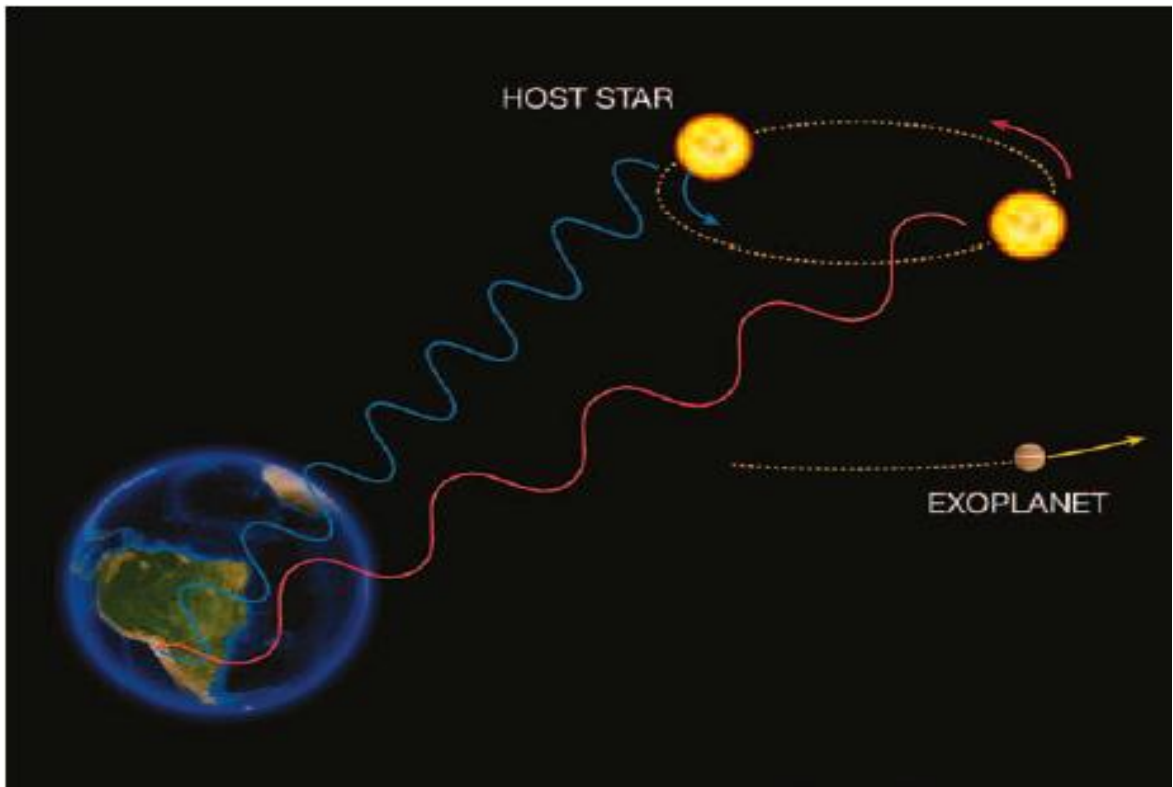
Figure 1.12 Doppler shifts caused by the periodic motion of a star around its system's barycentre. [Figure Credit: ESO Press Photo 22e/07 (http://www.eso.org/public/outreach/copyright.html); http://www.eso.org/public/images/eso0722e/; date of access: 16th of July 2012]

To specify, measuring Doppler shifts we find the velocity amplitude K of the star caused by a planet

$$K = (\frac{2\pi G}{P})^{1/3} \frac{M_p sin i}{(M_{star}+M_p)^{2/3}} \frac{1}{\sqrt{1-e^2}} \tag{1.1}$$

where P is the observed orbital period of the star, G the gravitational constant, e the eccentricity, i the inclination of the orbit of the planet to a line perpendicular to the line of sight and M_{star} and M_p the masses of the star and the planet respectively. Using Kepler's third law

$$P^2 = \frac{4\pi^2 a^3}{G(M_{star}+M_p)} \tag{1.2}$$

where α is the distance between the star and its companion, we can determine the semi-major axis and estimate the mass of the planet (Marcy et al. 1998; Cumming et al. 1999; Perryman 2000). However, the main problem with this technique is that we can actually determine only the minimum mass of the companion $M_p \times sini$, as we do not know its orbital inclination (Marcy et al. 1998; Perryman 2000; Santos 2008).

A limitation of the radial-velocity technique is that this technique is not appropriate for the detection of planets around young and active stars but is more applicable to late-type objects (Santos 2008). Another limitation of this technique, in regard to M dwarfs, is that that these objects are not bright enough to obtain for them enough data on time that usually spectrographs require (Reiners et al. 2010).

Finally, a lot of projects run with the aim to detect exoplanets with the radial-velocity technique like the California & Carnegie Planet Search (Crane et al. 2006) and the ELODIE spectrograph (Naef et al. 2004), which have led to the discovery of several exoplanets (Schneider 2012).

1.5.2 Astrometry

Similar to the radial-velocity technique, astrometry is based on the gravitational effects that a companion causes to its host star. To be more specific, in this technique we observe the different positions of a star while it is moving around its system barycentre (Marcy et al. 1998; Perryman 2000; Santos 2008).

For a star of mass M_1 and semi-major axis α_1 with a planetary companion of mass M_2 and semi-major axis α_2, the third law of Kepler gives:

$$P^2 = \frac{\alpha^3}{M_1 + M_2} \qquad (1.3)$$

where P, is the orbital period and $\alpha = \alpha_1 + \alpha_2$. Considering that

$$M_1 \alpha_1 = M_2 a_2 \qquad (1.4)$$

the semi-major axis α_1 of the star is equal to

$$\alpha_1 = \frac{M_2}{M_1 + M_2} \alpha. \tag{1.5}$$

Measuring the period P and the semi-major axes α_1 and α_2, we can determine the masses of the two objects M_1 and M_2 (Santos 2008).

Astrometry has the advantage that it can detect companions at larger distances from their host compared to the radial-velocity technique (Marcy et al. 1998) and with long orbital periods (Perryman 2000; Santos 2008).

Although a limitation of astrometry is that the stellar spots may affect the measurements (Lanza et al. 2008), we can minimise this problem by observing in the near-infrared, where the spots are not so visible (Santos 2008).

Surveys, which are using the astrometric technique, include CAPS (Carnegie Astrometric Planet Search) program (Boss et al. 2009) and PHASES (Palomar High-precision Astrometric Search for Exoplanet Systems) (del Burgo et al. 2010).

1.5.3 Transit Method

When a planet passes in front of a star (in the line-of-sight, observer-star) we can say that the planet transits its host star, reducing the star's luminosity (Figure 1.13). Considering a circular orbit, the probability P of a full transit in a planetary system is

$$P = \frac{R_S}{\alpha} \tag{1.6}$$

where α is the orbital radius (determined by Kepler's third law) and R_S the radius of the star (Santos 2008).
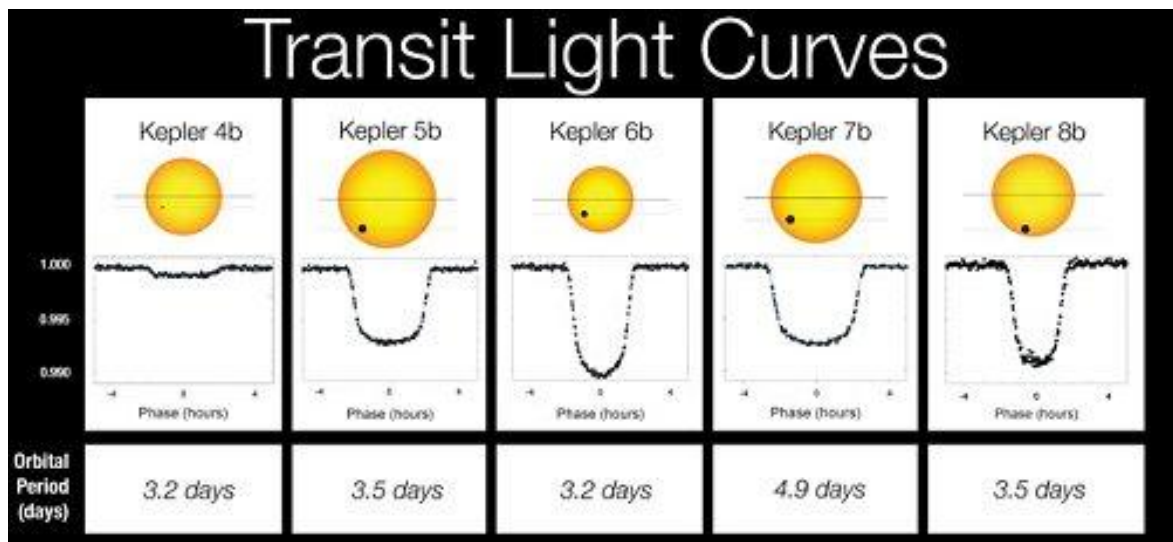
Figure 1.13   The photometric signature of five transiting planets. [Figure Credit: Science@NASA, http://science.nasa.gov/science-news/science-at-nasa/2010/04jan_fiveplanets/, date of access: 10th of June 2012]

In addition, the difference in the luminosity of a star, because of a transit, ΔL is equal to

$$\Delta L = \left(\frac{R_P}{R_S}\right)^2 L_S \tag{1.7}$$

where R_S and L_S are the radius and the initial luminosity of the star respectively and R_p the radius of the transiting planet (Figure 1.14) (Perryman 2000; Santos 2008).
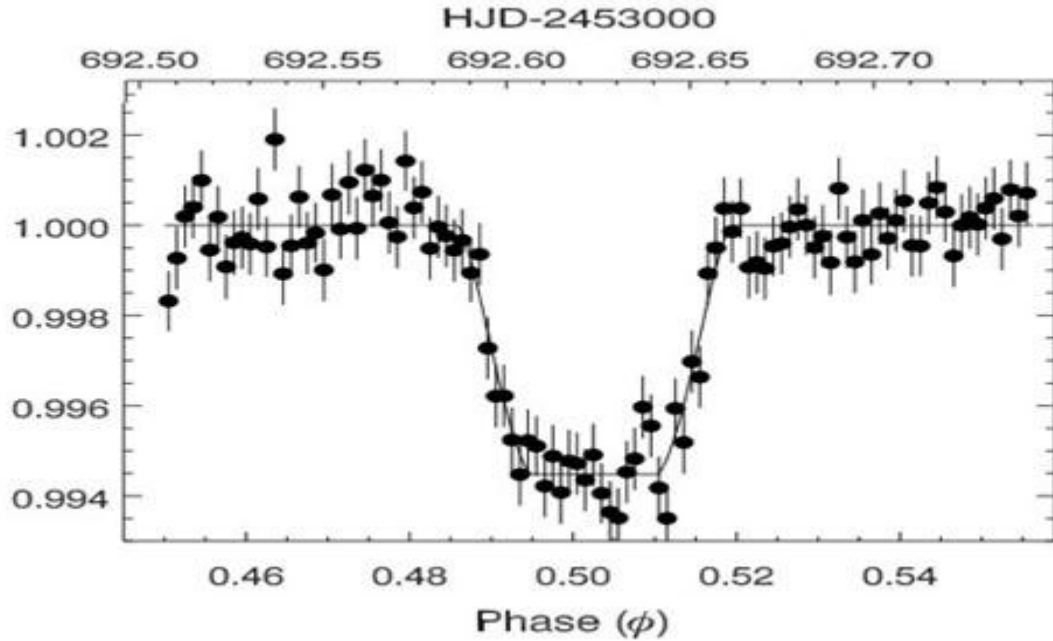
Figure 1.14 Thermal infrared emission from the transiting planet HD 189773b. At the vertical axis of the diagram we can see the relative intensity. [Figure Credit: AAS (http://iopscience.iop.org/0004-637X/page/Copyright+and+permissions); (Deming et al. 2006; p.562)]

Furthermore, the duration t of a transit in the ideal situation of an equatorial transit is

$$t = 13 \times R_S (\frac{\alpha}{M_S})^{1/2} \ days \tag{1.8}$$

where α is the orbital radius expressed in AU and R_S and M_S the radius and the mass of the star expressed in units of $R_\odot$ and $M_\odot$ respectively (Santos 2008).

Consequently, the transit method determines the radius and the orbital inclination of a planet and enhances the radial-velocity technique as these two methods combined provide us the exact mass and the orbital parameters of a planet (Pollacco et al. 2008; Santos 2008).

Moreover, planets that transit their parent star provide us information about their atmospheres and their chemical structure (Chabonneau et al. 2007).

Another important fact is that although the time between two successive transits can

be usually well determined, the presence of an additional planet in the particular system can cause that time to deviate from its expected value. As a consequence, it is possible to determine the orbit and the mass of a second planet in the same planetary system by just observing the first detected planet transiting its host (Holman et al. 2005).

A limitation of that method is that for objects of small mass ($<100M_{Jupiter}$), the photometric signature of the transiting planet is not sufficiently distinct, because of the flatness of the mass-radius relation (see e.g., Pont et al. 2005; Santos 2008).

One survey that is using the method of transits is WASP (Wide Angle Search for Planets) that started in 2006 (Butters et al. 2010). On the 6th of March 2009, NASA launched the Kepler mission, a space mission the purpose of which is to detect exoplanets with the method of transits and estimate the abundance of habitable planets (Borucki et al. 2010). There are also many other projects that use the method of transits for the discovery of extrasolar planets such as the CoRoT space mission, TrES (Transatlantic Exoplanet Survey) and Super WASP (Wide Angle Search for Planets), which continue to extend the catalogue of the discovered exoplanets (Schneider 2012).

1.5.4 Gravitational Microlensing

When a star passes through the line-of-sight of the observer and another, distant, source star, then the gravitational field of the first star acts as a lens and increases the apparent brightness of the source star (Paczynski 1996). In the case of the presence of a planet around the lens star, since that planet has its own gravitational field, it may act, when it is in a certain position, as an additional lens to the source star's brightness (Mao et al. 1991; Benett et al. 1996; Perryman 2006; Mao 2008). This effect is called gravitational microlensing because of the lensing object's small mass (the lens is small as compared to the regular strong gravitational lensing) and is applicable to the detection of extrasolar planets (Figure 1.15) (Mao et al. 1991; Miralda-Escudé 1996; Sahu 1997; Perryman 2006; Gaudi et al. 2008). The first exoplanet ever detected with this method was OGLE-2003-BLG-235/MOA-2003-BLG-53, in 2003 (Bond et al. 2004; e.g. Bond 2012).
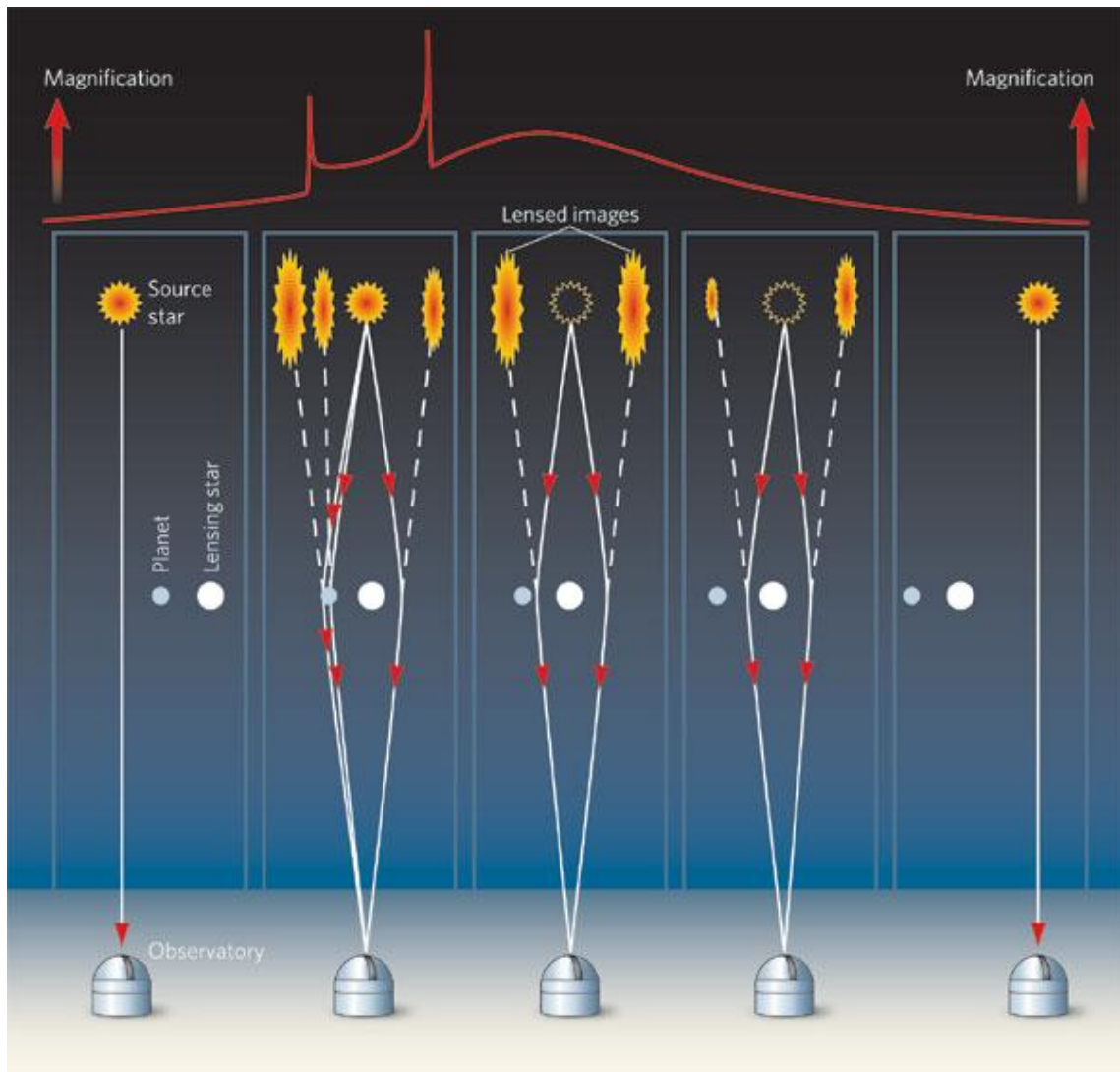
Figure 1.15 The gravitational microlensing effect. The red line shows the magnification of the source star's brightness according to the relative positions of the observer, the source star, the lens star and the planet that are presented in the Figure. [Figure Credit: Adapted by permission from Macmillan Publishers Ltd: [NATURE] (Queloz et al. 2006; p401), copyright (2006)]

Regarding the detection of exoplanets, gravitational microlensing is very sensitive to the detection of low mass planets (Beckwith et al. 1996; Benett et al. 1996; Sahu 1997; Perryman 2000; Beaulieu et al 2006) with large semi-major axis (Beaulieu et al 2006) around low mass stars (<0.25 $M_{\odot}$ that is the lower limit for the radial-velocity technique) (Benett et al. 2008). Consequently, this method can potentially reveal exoplanets in the habitable zone (Gould et al. 2010). Furthermore, gravitational microlensing is an efficient method in the discovery of exoplanetary systems with more than one planet (Gaudi et al.

2008; Mao 2008) and of exoplanets that are similar to the planets of our solar system (except for Mercury) (Gaudi et al. 2008). In addition, this method, because its sensitivity is independent of the lens luminosity, is applicable to the detection of planets in very distant orbits or even free floating planets (Han 2006, Bennett et al. 2007, Strigari et al. 2012).

A disadvantage of this method is that a microlensing effect is detected for a limited range of time (for few hours to few weeks, depending on the mass of the lensing object) since all the objects are moving and so, their relative position changes very fast (Yu et al. 1996; Sahu 1997). Furthermore, we are unable to repeat the same observation since it is very unlikely for the objects to be found for a second time in the exact position that is required for the observation of the microlensing effect (Yu et al. 1996). Thus, microlensing events are very rare (order of magnitude $\sim 10^{-6}$) and so, when we use microlensing as a method to detect exoplanets, it is necessary to observe repeatedly and simultaneously a large amount of source stars (Mao et al. 1991; Miralda-Escudé 1996, Paczynski 1996).

A more detailed description of the method of gravitational microlensing is given in Chapter 2.

1.5.5 Direct Imaging

Another method that is used for the detection of extrasolar planets is the direct imaging. By this term we mean the detection of light waves emitted by the exoplanet, originated either indirectly, through reflection from the parent star or directly, from the planet's inner thermal radiation (Perryman 2000; Rouan 2006; Traub et al. 2010).

The brightness of a planet L_P, for a specific wavelength λ, is defined by

$$\frac{L_P}{L_{star}} = \rho(\lambda, \alpha)(\frac{R_P}{\alpha})^2 \qquad (1.9)$$

where R_p is the radius of the planet, L_{star} the brightness of the host star, α the angle between the observer and the star as it is seen from the planet's perspective and $\rho(\lambda,\alpha)$ a phase-dependent function (Perryman 2000).

The observation of an exoplanet via direct imaging provides us important information about the planet, such as its temperature, the composition of its atmosphere and

its surface structure (Rouan 2006; Traub et al. 2010).

The main disadvantage of this method is the limited luminosity of the planets in regard to the luminosity of their host stars that hampers the observations (Marcy et al. 1998; Rouan 2006; Traub et al. 2010).

However, this limitation is being overcome as technology progresses and various projects are planned for the detection of exoplanets with direct imaging in the near future (Schneider 2012). Such projects, such as The Lyot Project (Sivaramakrishnan et al. 2007) and the VIDA (Vlti Imaging with a Densified Array) (Lardieere et al. 2008) are already running.

1.5.6 Pulsar Timing

Pulsar timing is a specific method for the detection of planets around pulsars. Similar to planetary systems around stars, the movement of a planet around a pulsar produces gravitational effects and as a consequence, the pulsar obtains its own orbital motion. Furthermore, the motion of the pulsar produces variations in the pulse timing that are easily detectable (Wolszczan 1997; Perryman 2000). Considering a circular orbit and a pulsar of mass $M_{pulsar} = 1.35 M_{\odot}$, the amplitude of timing residuals that originates from the planetary motion around the pulsar τ_p, is equal to

$$\tau_P = 1.2 \left(\frac{M_P}{M_{\oplus}} \right) \left(\frac{P_{orb}}{1yr} \right)^{2/3} ms \tag{1.10}$$

where *ms* denotes milli-seconds, M_p and P_{orb} are the mass and the orbital period of the planet respectively and $M_{\oplus}$ is the mass of the Earth (Wolszczan 1997).

Because of the precision of pulsar timing we are able to detect even very low mass planets around pulsars (Wolszczan 1997; Perryman 2000).

1.6 Extrasolar Planets and Planet Formation

The study of the physical properties of extrasolar planets and of their host stars may provide us important information for the formation of planetary systems (Tekenda et al. 2007).

The most popular theories for the mechanism of formation of planetary systems are the core-accretion model and the gravitational instability of gas hypothesis (Figure 1.16) (Gonzalez 1998; Udry et al. 2007).

According to the core-accretion model, terrestrial planets and the cores of gas giants are formed through accretion of planetesimals (solids of order of magnitude in the range of km or even larger (Youdin et al. 2002)) (Mizuno et al. 1980; Bodenheimer et al. 1986; Lissauer 1993; Pollack et al. 1996; Ikoma et al. 2000; Youdin et al. 2002; Alibert et al. 2011). These planets and the giants' cores possibly migrated to their present locations, close to their parent star, through gravitational interactions with their planetesimals' disk (Goldreich et al. 1980; Lin et al. 1985; Murray et al. 1998; Trilling et al. 1998). One great disadvantage of the core-accretion model is that it

Figure 1.16 The two most popular theories for the formation of the planets. [Figure Credit: NASA/ESA and A. Feild (STScI), http://www.spacetelescope.org/images/opo0319f/, date of access: 10th of June 2012]

is unable to explain the range of time that is required for the formation of a giant planet, since the lifetime of protoplanetary disks should be shorter (Alibert et al. 2005; Alibert et al. 2011).

However, the discovery of a giant planet (mass= (9.8±3.3) $M_{Jupiter}$) orbiting the young star TW Hydrae (age 8-10 Myr) indicates that giant planets may be able to form before the circumstellar disk scatters, since studies (Haisch et al. 2001; Carpenter et al. 2005; Cieza et al. 2007) have shown that the lifetime of a disk is about 10Myr after the formation of the star (Setiawan et al. 2008). Furthermore, the migration scenario gives an advantage to the core-accretion model as it predicts shorter timescales for the formation of giant planets (Alibert et al. 2005) and in addition can explain the presence of massive planets very close to their parent star (Murray et al. 1998; Trilling et al. 1998; Alibert et al. 2005).

Specifically, migration predicts three different fates for the planets; planets that migrate very fast towards their parent star and consequently disappear (class I), planets that migrate towards their host star, lose a part of their mass and stabilize in an orbit close to the star (class II) and planets that migrate to small distances from their original location, towards their parent star without losing any mass (class III) (Trilling et al. 1998). Moreover, the process of migration should underlie chaotic rules, which may explain the reason why the observed exoplanets seem so diverse (Laughlin et al. 2004).

On the other hand, the gravitational instability hypothesis claims that giant planets are formed from collapsed gaseous protoplanets (clumps of dust and gas), which have formed respectively from the proto-star's gravitational collapse (Boss 1997). Moreover, the gravitational instability scenario predicts shorter formation times for the giant planets than the core-accretion model does (Boss 1997). However, the large core of the transiting planet HD 149026b indicates that the gravitational instability scenario may not be able to explain the formation of this giant planet (Sato et al. 2005).

Another factor that seems to play a critical role in the mechanism of planet formation is the metallicity of the central star, as the stars that host gas giant exoplanets seem to be more metal-rich than the stars of the Solar Neighborhood (Laughlin 2000; Gonzalez et al. 2001; Santos et al. 2001; Udry et al. 2007). This happens probably because this high metallicity of the parent star leads to higher probability of formation of a gas giant planet around it (Laughlin 2000; Ida et al. 2004). However, there is no such relation for the stars that host ice giants, like Neptune, since these stars are not necessarily characterized by

high metallicity (Sousa et al. 2008). In addition, another parameter of exoplanets that may be related to the metallicity of their parent star is their period. Gonzalez (1997) indicates that short period planets form preferentially around metal-rich stars and the reason for that may be that the planets are forming faster by high metallicity clouds, which increase the metallicity of the star and enhance the prospects of planetary migration that places the planets in small orbits around their host (Murray et al. 1998; Laoughlin 2000).

Furthermore, the discovery of massive planets in small orbits around their parent star that have a significant coverage of escaping atomic hydrogen in their atmosphere (Vidal-Madjar et al. 2003), which depends on the temperature of the atmosphere, indicates that these planets actually could evaporate (Lecavelier des Etangs et al. 2004). For the estimation of the time range that is necessary for the total evaporation of a planet we need to determine the semi-major axis and the mass of the planet (Lecavelier des Etangs et al. 2004). However, the discovery of a planet in a small orbit around the post-red-giant star V391 Pegasi proves that planets can survive at small distances around a red-giant (Silvotti et al. 2007).

Another parameter of massive exoplanets, their radius, seems to be related to effects of irradiation (Chabonneau et al. 2007) as these effects can explain the big radius of some of the exoplanets (Bodenheimer et al. 2001; Baraffe et al. 2003; Bodenheimer et al. 2003; Burrows et al. 2007).

Planet formation theories usually refer to the formation of planets around a central star but what about the free floating planets that are not bound to any host? The formation process of these planets may differ from that of stars and brown dwarfs as there is a difference in the mass function (Sumi et al. 2011). Specifically, during the formation of a planetary system, gravitational instabilities caused by the interaction between two bound planets for a multiple planetary system (Rasio et al. 1996; Stevenson 1999; Veras et al. 2009; Barry et al. 2011) or between the planetary system and any neighbourhood stars close by (Sigurdsson 1992) may lead to the ejection of a planet (Zapatero et al. 2000). These processes should be completed in the short range of time of a few million years (Zapatero et al. 2000). Furthermore, according to Smith et al. (2001), for a distance of 50 AU from their parent star, about half of the exoplanets should be ejected in globular clusters, 25% in open clusters and less than 10% in young clusters. In addition, Sumi et al. (2011) indicates that the unbound planets may be twice as common as the stars in our Galaxy. Consequently, the observation of these distant objects, which are separated from brown dwarfs according to

the deuterium burning mass limit (Zapatero et al. 2000; Caballero et al. 2007) is an important project, as they may provide us important evidence for the formation of the planetary systems.

1.7 This Dissertation

Twenty years have passed since the first discovery of an extrasolar planet (Wolszczan et al. 1992). Nowadays, the progress of technology has led to the detection of new exoplanets on a regularly basis (Schneider 2012).

Gravitational microlensing is a method applicable to the detection of unbound planets and a Galactic free floating planet population has been claimed around one year ago with this method (Sumi et al. 2011). But are these detected planets actually unbound? Is there any possibility for these planets to appear as free floating but be in reality bound planets?

The main aim of this project is to test if there is such a possibility using simulations of binary lensing events. In Chapter 2, we present an overview of the method of gravitational microlensing and its application to the detection of exoplanets, along with present and future surveys that use it for this reason. In Chapter 3, we outline the procedure that we follow in our simulations, the results of which are presented and analyzed in Chapter 4. Chapter 5 contains the final conclusions of our work and the proposed future work that may have to be done in order to provide us more accurate results.

CHAPTER 2

GRAVITATIONAL MICROLENSING

2.1 Theory

When we (the observers) are perfectly aligned with the lens and source, the source star's light forms a ring- the Einstein Ring. The angular radius of this ring, that is named the angular Einstein radius (θ_E), is equal to

$$\theta_E = \sqrt{\frac{4GM_{lens}}{c^2 D}} \tag{2.1}$$

where G is the gravitational constant, c the speed of light, M_{lens} the mass of the lens and

$$\frac{1}{D} = \frac{1}{D_{lens}} - \frac{1}{D_{source}} \tag{2.2}$$

where D_{lens} and D_{source} are the distances to the lens and to the source respectively. The absolute scale of the angular Einstein radius is typically unknown (Gaudi et al. 2008). In the case of a single point lens, the light that comes from the source star is deflected by an angle α that equals to

$$\alpha = \frac{4GM_{lens}}{r_E c^2} \tag{2.3}$$

where r_E is the Einstein radius (see Equation 2.11) (Einstein 1936).

Furthermore, the lens equation for a point lens is

$$\bar{\eta} + D_{sl}\hat{\alpha} = \bar{\xi}\frac{D_{source}}{D_{lens}} \tag{2.4}$$

where $\bar{\eta}$ is the angular position of the source, $\hat{\alpha}$ the deflection angle, $\bar{\xi}$ the position of the image, and D_{sl} the distance between the lens and the source star. If we divide both sides of

the previous equation with D_{source} we obtain

$$\bar{\beta} + \bar{\alpha} = \bar{\theta} \tag{2.5}$$

where $\bar{\beta} = \bar{\eta}/D_{source}$, $\bar{\alpha} = \hat{\alpha} \times D_{sl}/D_{source}$ and $\bar{\theta} = \bar{\xi}/D_{lens}$ (Figure 2.1) (Mao 2008).
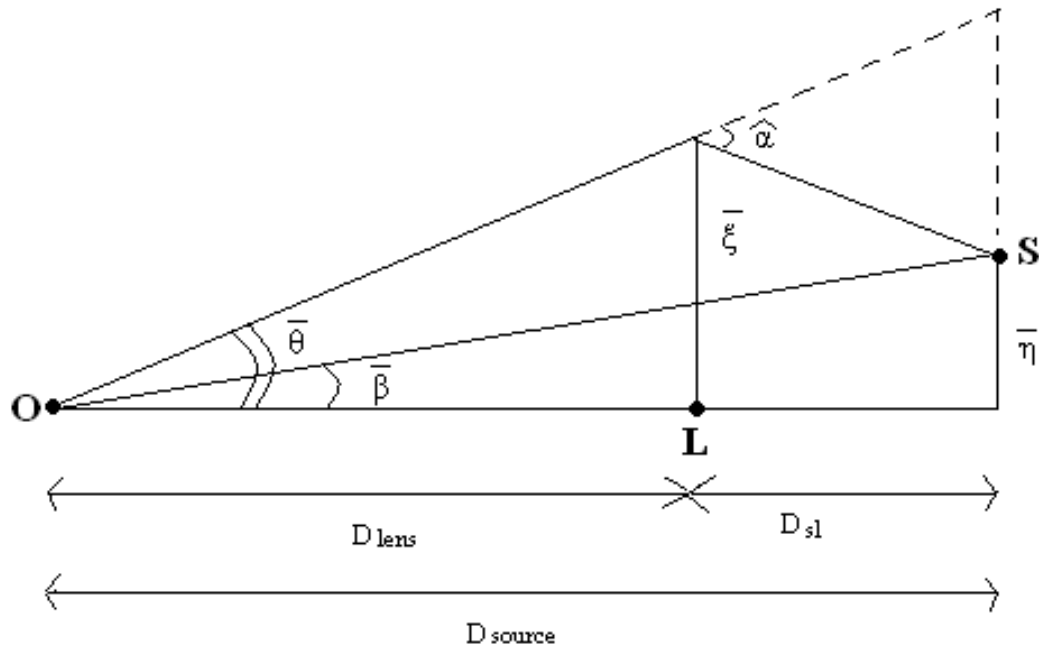
Figure 2.1 The geometry of the lens equation. The letters S, L and O indicate the position of the source star, the lens star and the observer respectively and D_{lens}, D_{source} and D_{sl} are the distances to the lens star, to the source star and between the lens and the source star respectively.

Assuming now that the mass distribution is axis-symmetric the vector sign can be ignored and thus

$$\beta + \alpha = \theta \tag{2.6}$$

(Mao 2008). Moreover, considering that the deflection angle is

$$\hat{\alpha} = \frac{\alpha G M_{lens}}{c^2 \xi^2} \bar{\xi} \tag{2.7}$$

where $\xi = D_{lens} \times \theta$ and the scaled deflection angle is

$$a = \frac{D_{sl}}{D_{source}} |\hat{a}| = \frac{\theta_E^2}{\theta} \tag{2.8}$$

the lens equation in angles can be written as

$$\beta + \frac{\theta_E^2}{\theta} = \theta \tag{2.9}$$

and by dividing both sides of the above equation with θ_E, we obtain

$$u + \frac{1}{u_1} = u_1 \tag{2.10}$$

where $u = \beta/\theta_E$ and $u_1 = \theta/\theta_E$ (Mao 2008).

In addition, if we determine the angular size θ_{source} of the source star (by measuring the source star's flux and determining its colour) we can find the Einstein radius (Yoo et al. 2004), since the lensing effect provide us in some cases the relative value $\rho = \theta_{source}/\theta_E$ (Gould 1994).

In addition, the Einstein radius' physical size is

$$r_E = \theta_E \times D_{lens} = \sqrt{\frac{4 G M_{lens} D_{lens} (D_{source} - D_{lens})}{c^2 D_{source}}} \tag{2.11}$$

or

$$r_E \approx 2.2 AU \sqrt{4 \times \frac{D_{lens}}{D_{source}} (1 - \frac{D_{lens}}{D_{source}})} \left(\frac{D_{source}}{8 kpc}\right)^{1/2} \left(\frac{M_{lens}}{0.3 M_\odot}\right)^{1/2} \tag{2.12}$$

(Gould 1992; Mao 2008).

Furthermore, we also define the Einstein radius timescale t_E, which defines the characteristic time that a microlensing event lasts and is equal to

$$t_E = r_E / v_t \tag{2.13}$$

where v_t is a relative transverse velocity of the lens and the source (Mao 2008).

In practice, we observe and measure from the ground only the magnification of the source star's brightness as a function of time (Mao 2008). This magnification $A(t)$ equals to

$$A(t) = \frac{u^2(t)+2}{u(t)[u^2(t)+4]^{1/2}} \tag{2.14}$$

where $u(t)$ is the impact parameter (angular distance between the source and the lens divided by θ_E) as a function of time and is equal to

$$u(t) = \sqrt{u_0^2 + \left(\frac{t-t_0}{t_E}\right)^2} \tag{2.15}$$

where u_0 is the minimum angular distance between the lens and the star (at $t=t_0$) divided by θ_E and t_0 is the time when the magnification peaks (Perryman 2000; Mao 2008).

The basic model parameters of single-lens gravitational microlensing are: the time t_0, the Einstein timescale t_E, the minimum angular distance (divided by θ_E) u_0, the baseline magnitude M_S and a blending parameter f_s, which refers to the part of the light that comes from the source star (Mao 2008).

In the case of a multiple lens system, which produces a more diverse light curve the lens equation becomes

$$\bar{u} = \overline{u_1} - \sum_{k=1}^{N} m_k \frac{\overline{u_1} - \overline{u_{1k}}}{|(\overline{u_1} - \overline{u_{1k}})|^2} \tag{2.16}$$

where $\overline{u_{1k}} = (x_{1k}, y_{1k})$ is the position of the lensing objects, $m_k = \frac{M_k}{M}$ the fraction of mass of N lensing objects and $\sum_{k=1}^{N} m_k = 1$ (Mao 2008) or

$$z = z_1 - \sum_{k=1}^{N} \frac{m_k}{\overline{z_1} - \overline{z_{1k}}} \tag{2.17}$$

where the complex quantities $z = x + yi$, $z_1 = x_1 + y_1 i$ and $z_{1k} = x_{1k} + y_{1k} i$ (Witt 1990). In this case the magnification is

$$A = J^{-1} \tag{2.18}$$

where J is the Jacobian of the mapping from the source to the lens plane, which equals to

$$J = \left| 1 - \frac{\partial z}{\partial \overline{z_1}} \frac{\overline{\partial z}}{\partial \overline{z_1}} \right| \tag{2.19}$$

(Witt 1990).

Moreover, the positions of the image that satisfy $J=0$ form continuous critical curves given by

$$\left| \sum_{k=1}^{N} \frac{m_k}{(\overline{z_1} - \overline{z_{1k}})^2} \right|^2 = 1 \tag{2.20}$$

In the source plane these curves are mapped as caustics (Mao 2008).

The model parameters in the specific case of a binary system are: the mass ratio $q=M_{planet}/M_{lens}$, the host-planet sky-projected separation s, the Einstein radius timescale t_E, the magnitude of the source star M_S, the time of closest approach to the centre of mass t_0, the minimum impact parameter u_0 and the trajectory angle between the source and the lens axis α (c.f. Bennett et al. 2008). If finite source size effects are important then the binary model must also take account of the source radius crossing time t_*. Additionally, if the parallax motion of the line of sight due to the binary system's orbit is significant then two additional parallax parameters are required (c.f. Bennett et al. 2008).

2.2 Microlensing Light Curves

By plotting the magnification as a function of time we produce a light curve, the shape of which depends on the stellar objects that cause the magnification of the source (Perryman 2000). Thus, as it can be seen in the Figure 2.2, for a single star that does not

host any planet (Figure 2.2a) we have a single lensing event and the light curve has just one wide peak and for a planet in a close orbit around the lens star (Figure 2.2b) we have a wide peak with a blip. For a planet in a distant orbit around the lens star (Figure 2.2c) we have a double lensing event (Figure 2.3). Finally, in the case of a free floating planet (Figure 2.2d), we have a single lensing event but in this case the peak is much narrower than it was in the first case.
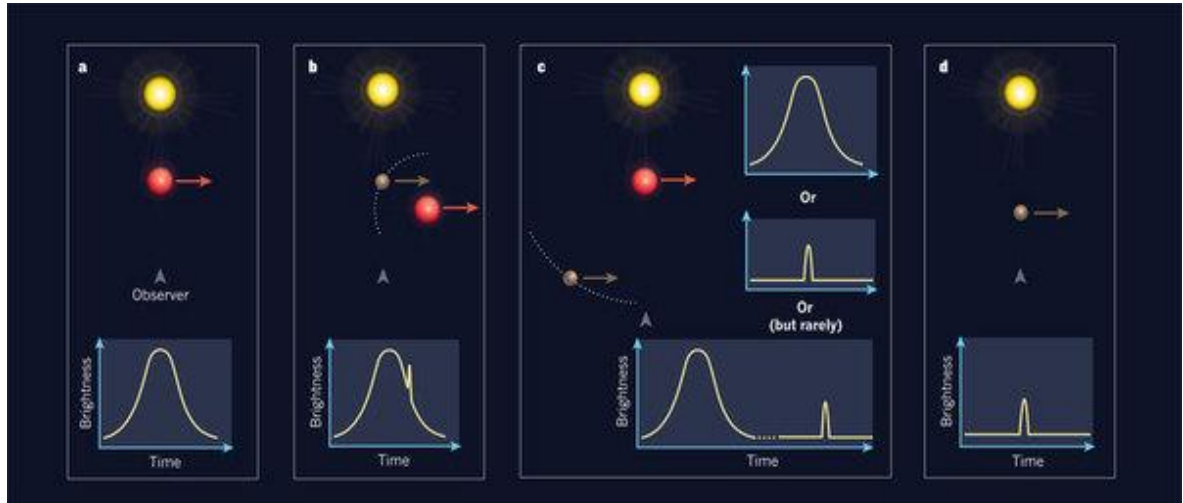
Figure 2.2 The characteristic light curves that we obtain when a lens star (red) passes in front of another distant source star (yellow) (a), when there is a planet (brown) in an orbit around the lens star (b), when the orbit of the planet around the lens star is distant (c) and when a planet is unbound (d). [Figure Credit: Adapted by permission from Macmillan Publishers Ltd: [NATURE] (Wambsganss 2011; p.290), copyright (2011)]

Figure 2.3 The light curve of a binary microlensing event. [Figure Credit: ESO Press Photo 17a/01 (http://www.eso.org/public/outreach/copyright.html); http://www.eso.org/public/images/eso0117a/; date of access: 16th of July 2012]

2.3 Microlensing Surveys

There are various surveys running in order to detect extrasolar planets. OGLE (Optical Gravitational Lensing Experiment) (Udalski et al. 2008) and MOA (Microlensing Observation in Astrophysics) (Sumi 2010) are the only projects searching for exoplanets via gravitational microlensing.

2.3.1 OGLE (Optical Gravtational Lensing Experiment)

The Optical Gravitational Lensing Experiment (OGLE) is a survey, which started twenty years ago in order to observe the dark matter using gravitational microlensing (Udalski et

al. 1997). To date, the first three phases of the project have already been concluded and the fourth is still running.

In 1992, started the project's first phase (OGLE-I) using the 1-m Swope telescope at the Observatory of Las Campanas in Chile (Udalski et al. 1997). This first phase, concluded in 1995 with great success including the discovery of the first microlensing event by a binary object (Udalski et al. 1994).

The second phase of the program (OGLE-II) started in 1996 using the new 1.3-m Warsaw Telescope (Figure 2.4 (left panel)) in the Las Campanas Observatory, operated by the Carnegie Institution of Washington (Udalski et a1. 1997), with main targets the Large Magellanic Cloud (LMC), the Small Magellanic Cloud (SMC), the Galactic Bulge and the Galactic Disk (Table 2.1) and concluded in 2000 (Soszynski 2006). Furthermore, follow-up projects such as the PLANET project, started using the data from the observations of OGLE in order to detect extrasolar planets (Jaroszynski et al. 2002).

Table 2.1 The main targets of the OGLE-II project and the
number of stars detected at each one of them.
[Udalski et al. 1997; p.342]

TARGET	LMC	SMC	Galactic Bulge	Galactic Disk
Field area (Sq. Degrees)	4.2	2.3	10	0.7
Number of Stars	7×10^6	2×10^6	30×10^6	0.6×10^6

The third phase of OGLE (OGLE-III) started the 12th of June in 2001 with the same telescope but with a ew eight-chip mosaic CCD camera (Udalski et al. 2002) and concluded in 2009 (Wyrzykowski et al. 2011) and its contribution in the detection of exoplanets was significant (Udalski 2009).

The fourth phase of the OGLE project started in 2010 with a new 32-chip mosaic CCD camera (Udalski 2009) and is still running till today.

The observations of the OGLE project led to the discovery of the OGLE-TR-56, which is the first exoplanetary system that has been discovered with the transit method

(Konacki et al. 2003) and, in collaboration with the MOA group, to the first discovery of an exoplanet with the method of gravitational microlensing (Bond et al. 2004; Bond 2012). To date, OGLE, has contributed to the detection of 15 exoplanets, 8 of them with the method of transits and 7 with the method of gravitational microlensing (Schneider 2012).

2.3.2 Microlensing Observation in Astrophysics (MOA)

MOA (Microlensing Observation in Astrophysics) is a survey for the detection of exoplanets with the method of gravitational microlensing, which started in 1995, using the 61-cm telescope at Mt. John observatory in New Zealand (MOA-I). This telescope was replaced by a new 1.8-m telescope (Figure 2.4 (right panel)) with an 8k x 10k-pixel CCD camera in 2005 (MOA-II) (Sumi 2010).
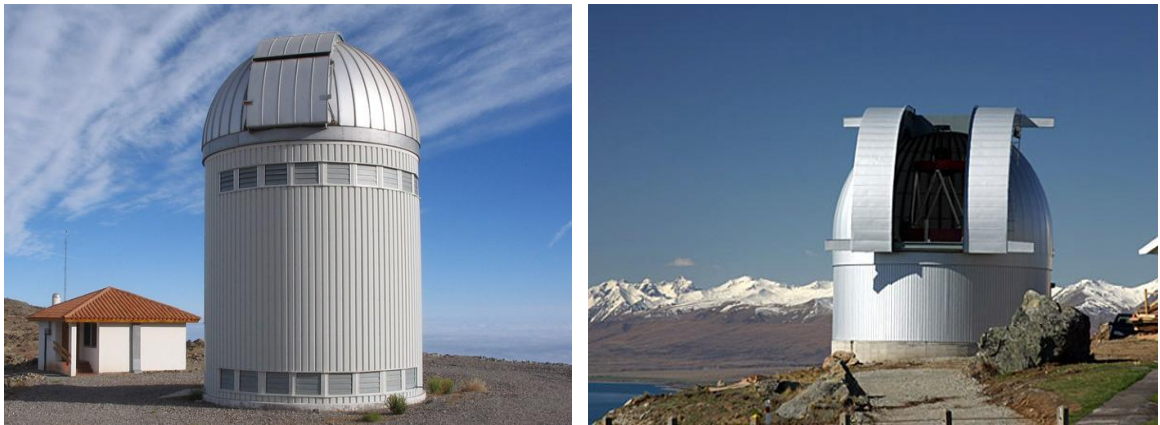
Figure 2.4 left panel: The 1.3-m Warsaw Telescope at Las Campanas Observatory, Chile. [Figure Credit: OGLE; http://ogle.astrouw.edu.pl/cont/7_photogallery/gallery_lco.php; date of access: 16th of July 2012], right panel: The 1.8-m telescope at the Mt. John observatory in New Zealand. [Figure Credit: MOA; http://www.phys.canterbury.ac.nz/moa/IMG_4998.jpg; date of access: 14th of July 2012]

Like OGLE, MOA reduces its data in real time and if a signal from a planet is detected, MOA takes imaging observations with high resolution, using VLT (Very Large Telescope) and Keck telescopes, in order to separate the lens and the source star from the other stars and to determine the mass of the lens star (Sumi 2010).

To date, 9 exoplanets has been detected by MOA and one with the collaboration of MOA and OGLE (Schneider 2012).

2.4 Future Missions

The realization of the importance of gravitational microlensing in the detection of extrasolar planets and the progress of technology, has given rise to the development of future ground and space-based surveys, which will use the method of gravitational microlensing in order to detect exoplanets, planned by many different organizations like ESA and NASA.

2.4.1 Korea Microlensing Telescope Network (KMTNet)

KMTNet (Korea Microlensing Telescope Network) is a future project of KASI (Korea Astronomy and Space Science Institute), the planning of which started in 2009 and its target is to detect exoplanets via microlensing. For this purpose, three different wide-field telescopes will be constructed, one in Chile, one in South Africa and one in Australia, which will observe near the Galactic Bulge (Kim et al. 2010).

The observations of this project are expected to start in 2014 (Kim et al. 2010).

2.4.2 Antarctic Schmidt Telescopes (AST3)

AST3 (Antarctic Schmidt Telescopes) is a future project that includes in its scope the search for exoplanets with the gravitational microlensing technique, proposed by CCAA (Chinese Center of Antarctic Astronomy) (Cui et al. 2008; Yuan et al. 2010). For the purposes of this project, the Chinese astronomical community planned to build three telescopes of 50 cm aperture each, in the location of Dome A in Antarctica (Cui et al. 2008).

2.4.3 EUCLID

EUCLID is a space mission supported by ESA that includes in its plans the detection of exoplanets via gravitational microlensing. The telescope of that mission is planned to have a diameter of 1.2 m and to observe at the optical and near-infrared optical windows (Beaulieu et al 2010). Particularly, observations at the near-infrared are expected to support the detection of exoplanets around mid- and late-M stars (Reiners et al. 2010).

The prospect of that mission, concerning the exoplanet search, is to provide statistical results of free floating planets and habitable planets with small masses ($\geq M_{Mars}$) in the first three months of its observations of Galactic Buldge and determine accurate analogues of habitable planets of 1 $M_{\oplus}$ mass that orbiting solar type stars in the following 9 months (Beaulieu et al 2010).

As soon the results of EUCLID get combined with the results of Kepler and of radial-velocity surveys we will be able to have an absolute clear statistical view of all types of exoplanets even of those with very small masses (Beaulieu et al 2010).

2.4.4 Wide Field Infrared Survey Telescope (WFIRST)

The NASA's planned space mission WFIRST (Wide Field Infrared Survey Telescope) that will make observations at near infrared, is a project that includes in its purposes the search for exoplanets with the microlensing technique. This exoplanet survey that will observe for 500 days in a range of time of 5 years will provide us statistics that will give a complete picture of, even habitable and free floating planets with small masses ($\geq 0.1\ M_{\oplus}$) (Barry et al. 2011). This prospect is very important because it is impossible to detect small ($\approx M_{\oplus}$) free floating planets from ground based observations (Barry et al. 2011).

Moreover, the expected results of the exoplanet survey of WFIRST are the detection of 3250 exoplanets around stars, 320 of which will be smaller than the Earth and 2080 free floating planets, 190 of which will have a mass smaller than that of the Earth (Barry et al. 2011).

CHAPTER 3

MICROLENSING LIGHT CURVES MODELLING

3.1 Introduction

As mentioned in Section 2.2, the light curve of a free floating planet is usually different from that of a bound planet, as in the first case we have a single lensing event and in the second a binary lensing event. But the light curve of a free floating planet is also different from that of a single star with no planets in an orbit around it; although that in both cases we have a single lensing event, in the second case the peak is typically much wider, since the event for a star lasts for a longer time (days or weeks) than for a planet (few hours to few days) (Yu et al. 1996).

But how accurate are these assumption in real observations? Is it possible that for some specific parameters of the lens star, the source star and the planet, a bound planet can appear as a free floating one? In the following sections we describe how we can test if there is such a possibility by modelling binary lensing events.

3.2 Binary Lensing Event Modelling

Our aim is to produce light curves of binary lensing events for various parameters for the source star, the lens star and the planet and to determine if there are any combinations of them for which a bound planet can appear as a free floating one. In order to produce these light curves we generate these parameters by using a simulation program, which have been developed in python.

Catalogue of Stars

We use a catalogue of stars generated from the synthetic microlensing catalogues of Kerins et al. (2009) based on the Besancon Galactic model (Robin et al. 2003; Marshall et al. 2006), which represents the statistical properties of real stars and provide us 93763 different

combinations of values for the mass M_L and the distance D_L of the lens star in units of $M_\odot$ and kpc respectively, the distance D_S in units of kpc and the magnitude M_S of the source star, the transverse velocity v_t in units of km/sec, the largest impact parameter (angular distance between the lens and the source star divided by θ_E), which allows the source to be brightened above the assumed survey limit (I=19 mag (see next paragraph)) u_{max} and the statistical weight wg in each case. The statistical weight is used to rate-weight the simulation results and is proportional to the rate of an event and a product of the lens Einstein Radius, the lens-source transverse velocity and the u_{max} (Kerins et al. 2009).

To specify, this catalogue is a simulation of stars generated from the Besancon Galactic model, with a fixed representative direction ($|l| < 100^o, |b| < 10^o$) (Marshall et al. 2006), for an I-band survey such as OGLE and MOA, which assumes a survey limit of I=19 mag (Kerins et al. 2009). Moreover, as mentioned before, the total number of source-lens pairs that are simulated in the catalogue is 93763.

Furthermore, the underlying Galactic model includes a Bulge, a thin disk with seven distinct populations of different age, a thick disk and a stellar halo (Robin et al. 2003).

Developing the Program in Python

We generate the time to start calculating the magnification t_{start} as 0 days and the time to stop calculating the magnification t_{end} as 283.7 days in order to simulate a typical MOA observing season (time data came from: MOA[5]).

Furthermore, we generate random parameters for the time when the magnification has the maximum value t_0, from t_{start} to t_{end} and for the minimum impact parameter u_0, from 0 to u_{max} (for $u_0 > u_{max}$ the magnification will not be visible and so, this case does not interest us). Moreover, we generate random parameters for the host-planet sky-projected separation s (a lower limit to the true host-planet orbital separation), logarithmically sampled from 0.1 to 100 AU (considering our Solar System, we can argue that between this range a planet should be certainly bound to its host) and for the angle between the lens trajectory and the line between the host and the planet α, from 0 to 2π radians (all possible angles). For the mass of the planet M_p we use 9 different logarithmically sampled values from 1 $M_\oplus$ to 10000 $M_\oplus$ (1 $M_\oplus$, 3.1623 $M_\oplus$, 10 $M_\oplus$, 31.623 $M_\oplus$, 100 $M_\oplus$, 316.23 $M_\oplus$, 1000 $M_\oplus$,

3162.3 $M_\oplus$, 10000 $M_\oplus$), since the 10000 $M_\oplus$ is considered to be the deuterium-burning lower limit and thus, the biggest mass that planets can achieve (Saumon et al. 1996).

Now we convert the mass of the lens to units of Earth masses and we calculate the mass ratio

$$q = \frac{M_p}{M_L} \tag{3.1}$$

Moreover, we calculate the Einstein Radius r_E using the equation 2.11 and the Einstein timescale t_E by equation 2.15, which we convert to units of days. Finally, we convert the host-planet sky-projected separation to units of r_E ($d=s/r_E$) and the angle α from radians to degrees ($\theta = \frac{a \times 180}{\pi}$).

After generating the parameters, we use a program in c$_{++}$, which takes as input parameters the mass ratio q, the time of peak magnification t_0, the sky-projected separation d, the Einstein timescale t_E, the angle θ, the minimum impact parameter u_0, the t_{start} and the t_{end} and provides us the binary magnification $A(t)$ as a function of time. To specify, this program generates the time t (days) between t_{start} and t_{end} and considering that the origin is the centre of mass, calculates the position $(u_0 \times \theta - \frac{t-t_0}{t_E} \times \sin(\theta),\ u_0 \times \sin(\theta) + ((t-t_0)/t_E) \times \cos(\theta))$ of the source star for each t, the position, ($d/(1+q)$, 0) of the secondary lensing object (in our case the planet) considering it to be on the positive x-axis and the position $\left(\frac{-q \times d}{1+q}, 0\right)$ of the primary lensing object (in our case the lens star). Furthermore, it converts the position of the source star into a 2-dimensional complex position vector z using equation 2.19 and finally calculates the magnification A for each t using the equations 2.20 and 2.21. In addition, this program provides the caustics and the critical curves of the event.

Now, from the output of the c$_{++}$ program we use again python and we interpolate the values of the magnification using realistic values of observation times in order to simulate real time observations. In this project we use two different observation times (time samples), one of (a) standard cadence (time data came from: MOA[6]; MOA 2012-BLG-306) and one of (b) high cadence (time data came from: MOA[6]; MOA 2012-BLG-063).

Continuing, for each value of magnification, we calculate the theoretical magnitude

---

[6] https://it019909.massey.ac.nz/moa/alert/, [date of access: 14th of July 2012].

M_{th} of the source star as a function of time

$$M_{th}(t) = M_S - 2.5 \times \log_{10} A(t) \tag{3.2}$$

and its error

$$\delta M_{th}(t) = 0.1 \times 10^{0.2 \times (M_{th}(t) - 19)} \tag{3.3}$$

(the minimum magnitude error that we use is 0.01) and using Poisson deviates we generate statistically random values for the magnitude $M(t)$ of the source star as a function of time and we produce the light curve for the binary lensing event.

The t_0 is determined with respect to the centre of mass of the planetary system but in order to determine the origin of the peak of the light curve we also need to calculate the $t_{0(planet)}$ and the $t_{0(host)}$ for the planet and for the host star respectively. For events, which look like single-lens systems, if the curve peaks close to $t_{0(planet)}$, then the origin of the light curve is considered to be the planet and on the contrary, if the curve peaks close to $t_{0(host)}$, then the origin of the light curve is considered to be the host star. As mentioned before, we know the exact position of the planet and of the host star with respect to the centre of mass and thus, we can determine their distances from it. Hence, the distances of the planet (d_p) and of the host star (d_h) from their centre of mass are $d_p = \frac{d}{1+q}$ and $d_h = \frac{q \times d}{1+q}$ respectively, both in units of r_E. Furthermore, using simple geometry (Figure 3.1), we can calculate the distance L between A and B, in units of r_E, which is equal to

$$L = \frac{d}{\cos \alpha} \tag{3.4}$$

and thus, the time required to cross L in units of t_E is equal to $L \times t_E$. In the same way, we can determine the difference between t_0 and $t_{0(planet)}$ and between t_0 and $t_{0(host)}$ as

$$t_{0(planet)} - t_0 = d_p \times \cos alpha \times t_E \tag{3.5}$$

and

$$t_0 - t_{0(host)} = d_h \times \cos alpha \times t_E \tag{3.6}$$

respectively. We find the $t_{0(planet)}$ and $t_{0(host)}$ to be

$$t_{0(planet)} = \frac{d}{1+q} \times \cos alpha \times t_E + t_0 \qquad (3.7)$$

and

$$t_{0(host)} = t_0 - \frac{q \times d}{1+q} \times \cos alpha \times t_E \qquad (3.8)$$

respectively.
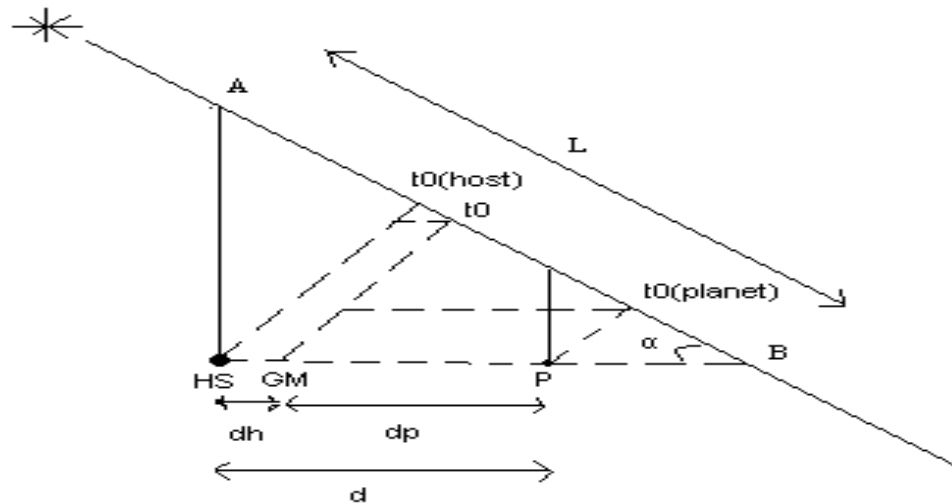
Figure 3.1 The relative positions of the centre of mass GM, the host star HS, the planet P, the t_0, the $t_{0(host)}$ and the $t_{0(planet)}$.

3.3 Single Lensing Event Fitting

We need to determine if our light curve is similar to the light curve of a single lensing event or if it shows its true binary origin. For this reason, we fit our light curve to a single lens model, using a least square fitting routine where

$$u(t) = \sqrt{u_0^2 + (\frac{t-t_0}{t_E})^2} \tag{3.9}$$

$$A_{fit}(t) = \frac{u^2(t)+2}{u(t)[u^2(t)+4]^{1/2}} \tag{3.10}$$

$$M_{fit}(t) = -2.5 \times log_{10}\left(A_{fit}(t)\right) + M_S \tag{3.11}$$

The values used to initiate the fitting routine are equal to $u_{0(init)} = u_0 \times 1.0001$, $t_{0(init)} = t_0 + 0.5$, $t_{E(init)} = t_E \times 1.2$ and $M_{S(init)} = M_S \times 1.1$. We use values close to the true parameter values in order to ensure that we are located close to the true global minimum. We are not trying to test the robustness of the fitting algorithm but we do wish to see the effect of fitting errors due to photometric errors and cadence, which we should be able to achieve by seeding our initial guess close to the true values.

From the output of the least square fitting, we determine the fitting parameters $u_{0(f)}$, $t_{0(f)}$, $t_{E(f)}$ and $M_{S(f)}$ and the covariance cov, which is a 4x4 matrix. From the covariance matrix we calculate the errors of the fitting parameters $\delta u_{0(f)}$, $\delta t_{0(f)}$, $\delta t_{E(f)}$ and $\delta M_{S(t)}$ as the square roots of $cov_{1,1}$, $cov_{2,2}$, $cov_{3,3}$ and $cov_{4,4}$ respectively. In order to reflect the systematic error in photometry (photometric error$\geq$ 0.01 mag), we consider as minimum value for the magnitude of 0.01.

Now, in order to determine if we have a good fitting, we calculate the reduced chi-squared

$$\chi_r^2 = \frac{\Sigma_i(\frac{M(t)-M_{fit}(t)}{\delta M_{th}(t)})^2}{N-N_{power}} \tag{3.12}$$

where N is the total number of observations and N_{power} the degrees of freedom of the fitting, which in our case equals to 4.

Finally, we apply all the previous steps to all stars of the catalogue, for the nine planet mass-values, for both time samples of different cadence.

3.4   Rejection of Events

Now we have to exclude from our results events that do not satisfy some specific criteria. Firstly, we reject, for each planet mass case, four events, which are flagged in the input stellar catalogue as having a zero or negative value of t_E (the statistical weight for these cases is equal to zero). These result from occasional errors in the catalogue generation. Furthermore, we reject some rare cases of events for which the binary c_{++} program fails to calculate the magnification. Moreover, we reject some events, for which python fails to calculate the covariance after the fitting (typically we encounter a singular matrix which indicates extremely flat curvature in a certain direction).

Moreover, we have to exclude events for which the number of points in the range $(t_{0(f)} - t_{E(f)}, t_{0(f)} + t_{E(f)})$ is less than five, because in these cases the light curve is not sufficiently well defined. Furthermore, we exclude events, for which the number of points in the range $(t_{0(f)}, t_{0(f)} + t_{E(f)})$ or in the range $(t_{0(f)} - t_{E(f)}, t_{0(f)})$ is less than two in order to exclude cases where the peak of the light curve is outside from the time range of our simulations.

In addition, we have to exclude from our results events for which the reduced chi-squared is less than 0.5 (real observations of this kind are usually interpreted as having overestimated errors) and between 2 and 5, because these cases are borderline in terms of showing a clear binary signal, which is distinguishable from a single lens event.

Furthermore, we exclude from the total of the single lensing events the events for which $\left| t_{0(host)} - t_{0(planet)} \right| < 10 \times \delta t_{0(f)}$, because in these cases $t_{0(f)}$ is close to both the planet and the host star and thus, we cannot decide if the peak comes from the planet or from the host. Additionally, we exclude from the total of the single-like lensing events, the events for which $\left| t_{0(f)} - t_{0(planet)} \right| > 3 \times \delta t_{0(f)}$ and $\left| t_{0(f)} - t_{0(host)} \right| > 3 \times \delta t_{0(f)}$ because in these cases $t_{0(f)}$ is far from both the planet and the host star. This is normally indicative of the effects of a binary signal.

In Table 3.1 we can see how many events were excluded for each one of the above reasons, for each one of the nine values for the mass of the planet, for the standard and for the high cadence time sample.

Table 3.1 The number (*No*) of events that were excluded from our results, for the two time samples of different cadence (**a.** standard cadence, **b**. high cadence), for each planet mass value, for the following reasons: (**I**) the c_{++} program fails to calculate the magnification, (**II**) python fails to calculate the covariance, (**III**) the number of points between $t_{0(f)} - t_{E(f)}$ and $t_{0(f)} + t_{E(f)}$ is less than 5, (**IV**) the number of point between $t_{0(f)}$ and $t_{0(f)} + t_{E(f)}$ is less than 2, (**V**) the number of point between $t_{0(f)} - t_{E(f)}$ and $t_{0(f)}$ is less than 2, (**VI**) $\left| t_{0(host)} - t_{0(planet)} \right| < 10 \times \delta t_{0(f)}$, (**VII**) $\left| t_{0(f)} - t_{0(planet)} \right| > 3 \times \delta t_{0(f)}$ and $\left| t_{0(f)} - t_{0(host)} \right| > 3 \times \delta t_{0(f)}$, (**VIII**) the reduced chi-squared is between 2 and 5. The total number of rejected events is shown in the **Sum** column. As flagged as equal or less than zero in the input Besancon stellar catalogue and we have not encountered any case with reduced chi-squared less than 0.5. The total number of simulated events is 93763.

a. Standard Cadence Time Sample									
		Reason For Excluding Event							
		I	II	III	IV	V	VI	VII	VIII	Sum
		(*No*)	(*No*)	(*No*)	(*No*)	(*No*)	(*No*)	(*No*)	(*No*)	
	1	4	299	703	1753	617	14006	1590	321	19297
	3.1623	1	285	713	1788	634	13859	2255	293	19829
	10	1	277	646	1747	660	14076	4759	345	22515
Plan.	31.623	2	292	684	1783	618	13972	10444	357	28156
Mass	100	0	252	663	1682	626	13952	19880	387	37446
($M_\oplus$)	316.23	0	130	847	1845	790	14108	30492	471	48687
	1000	0	89	1752	2159	1129	14451	39696	676	59965
	3162.3	0	95	4818	2690	1758	15865	43759	1208	70197
	10000	0	97	9162	3231	2467	18586	45104	1900	80551

b. High Cadence Time Sample									
		Reason For Excluding Event							
		I	II	III	IV	V	VI	VII	VIII	Sum
		(No)	(No)	(No)	(No)	(No)	(No)	(No)	(No)	
	1	2	272	589	1685	472	10271	2142	332	15769
	3.1623	4	281	578	1645	456	10408	3388	308	17072
	10	0	314	624	1719	481	10423	7034	329	20928
Plan.	31.623	3	289	566	1524	454	10334	14641	384	28199
Mass	100	2	232	588	1633	518	10401	25460	356	39194
($M_\oplus$)	316.23	0	111	698	1644	629	10535	37198	469	51288
	1000	0	81	1337	2033	974	10825	46698	744	62696
	3162.3	0	90	3706	2895	1990	11646	51070	1193	72594
	10000	0	86	7323	3785	2943	13515	52544	1957	82157

3.5 Free Floating Planet Selection Criteria

We now show how we can determine if the light curve of a binary lensing event is similar to the light curve of a free floating planet.

As mentioned before, in real observations the light curve of a free floating planet should fit well to the light curve of a single lensing event and have a very narrow peak (few hours to few days). Furthermore, for our simulations, as we simulate by definition binary lensing events, it has to be assumed that the light curve of a free floating planet-like microlensing event should peak close to $t_{0(planet)}$

If the reduced chi-squared χ_r^2 in our simulations is between 0.5 and 2, then we can say that we have a good fit and that means that the light curve of our model of the binary lensing event is very similar to the light curve of a single lensing event and thus, is similar to the light curve of a single star with no bound planets around it or to the light curve of a free floating planet with no obvious contribution from the host. On the contrary, if the χ_r^2 is larger than five we can argue that the light curve of our model should be a binary lensing event light curve (we have already excluded from our results the cases where $\chi_r^2<0.5$ and $2<\chi_r^2<5$).

In addition, if the width of the peak $t_{E(f)}$ is small enough ($t_{E(f)}<5days$) and $t_{0(f)}$ is close to $t_{0(planet)}$ ($\left|t_{0(f)} - t_{0(planet)}\right| < 3 \times \delta t_{0(f)}$), we can assume that our light curve is similar to the light curve of a free floating planet.

In the cases of single lensing events, where $t_{0(f)}$ is close to $t_{0(planet)}$, but the width of the peak is longer than five days then, in our simulations, we assume that the event would not be recognised as a free floating planet, even though it could be one that is, e.g. moving very slowly across the line of sight.

Summarizing, if the calculated reduced chi-squared χ_r^2 is between 0.5 and 2, the $t_{E(f)}$ is smaller than 5 days and the difference between $t_{0(f)}$ and $t_{0(planet)}$ is smaller than $3 \times \delta t_{0(f)}$ we can assume that our binary lensing event light curve is very similar to that of a free floating planet and thus, we cannot differentiate them.

Moreover, we determine the parameters, for which the light curves of our model satisfies the above criteria. In Figure 3.2(a,b) we can see some examples of free floating planet-like microlensing light curves from our simulations.

Finally, we determine the parameters, for which the light curves seem to come from

the main host star (χ_r^2 is bigger than 0.5 and smaller than 2 but $\left|t_{0(f)} - t_{0(host)}\right| < 3 \times$ $\delta t_{0(f)}$ or $t_{E(f)}$>5) and the parameters, for which the curves are similar to them of binary lensing events (χ_r^2 is larger than 5). In Figures 3.2(c,d) and 3.2(e,f) we can see some examples from our simulations of microlensing light curves that seem to come from the main host star and binary-like microlensing light curves respectively.

As can been seen in the Figure 3.2(b) and the Table 3.2 a bound planet can appear as a free floating one even for projected separations as small as 4 AU. In the particular case of the microlensing event of the Figure 3.2(b) the sky-projected separation is still as twice the Einstein radius of the host star, which means that the host star contributes only a few percent of the magnification.

Table 3.2 The parameters that define the light curves of the Figure 3.2.

	Microlensing Event					
	a	b	c	d	e	f
time sample (cadence)	standard	high	standard	high	standard	high
$M_p(M_\oplus)$	1000.00	10000.00	10.00	100.00	3162.30	3.16
D_S(kpc)	8.05	8.53	12.53	8.39	11.83	9.59
D_L(kpc)	6.07	7.09	7.55	7.89	8.87	6.51
M_S	20.64	19.62	19.99	17.55	19.31	22.1
$M_L(M_\odot)$	0.14	0.31	0.11	0.11	0.11	0.11
v_t(km/sec)	462.70	306.15	903.43	328.57	873.89	245.6
t_0(days)	220.30	29.30	233.60	118.10	149.20	168.00
u_0	0.31	0.90	0.15	0.54	0.15	0.02
s(AU)	37.98	4.09	4.62	1.19	1.60	0.51
a(radians)	1.55	5.33	1.15	2.53	5.13	1.81
χ_r^2	0.92	1.14	0.96	0.99	12.55	14.02
$t_{0(planet)}$(days)	223.77	41.60	269.86	113.00	160.96	167.12
$t_{0(host)}$(days)	220.21	28.12	233.59	118.10	148.23	168.00
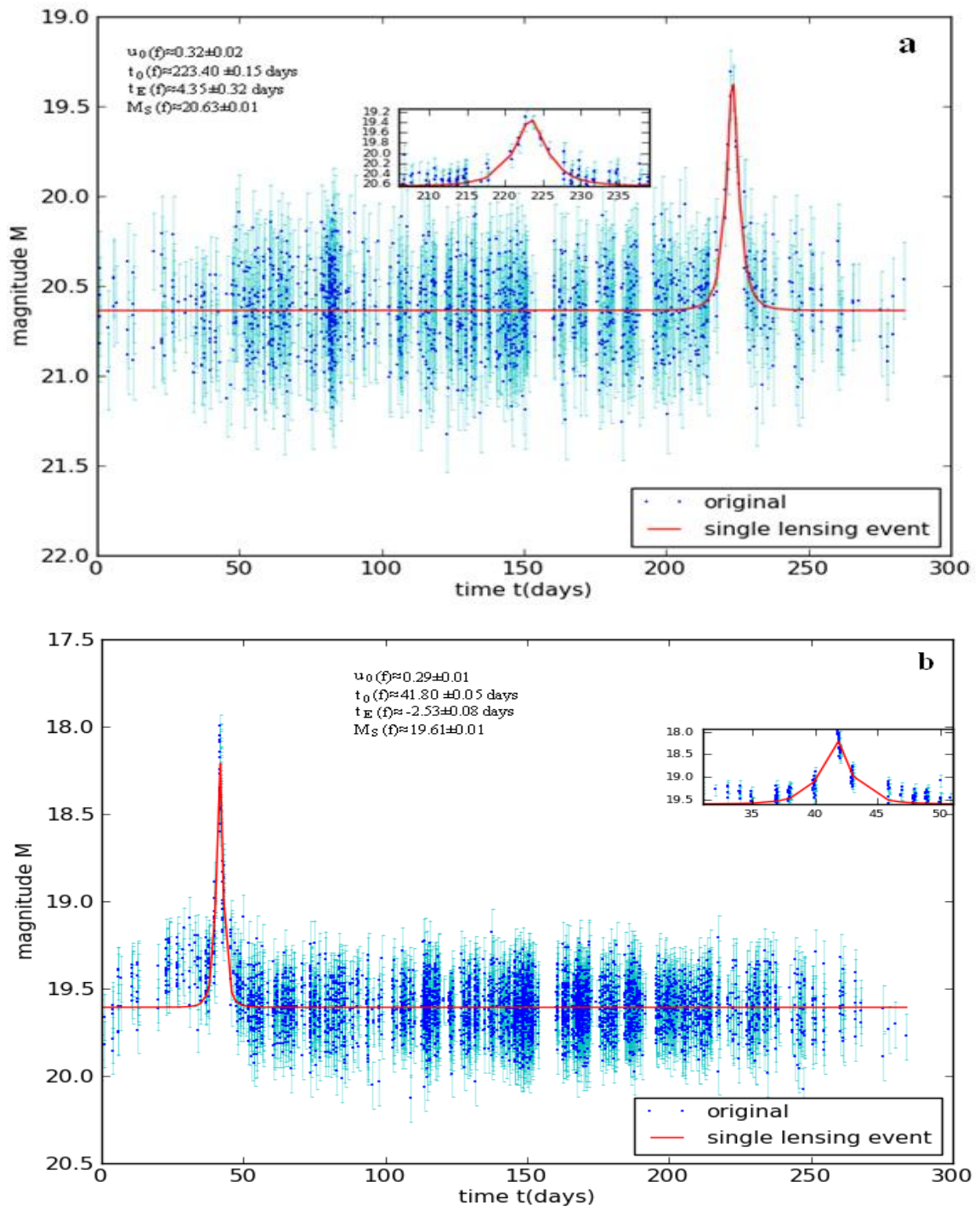
Figure 3.2 Microlensing light curves of free floating planet-like microlensing events (**a,b**), microlensing light curves that seem to come from the host star (**c,d**) and microlensing light curves of binary-like microlensing events (**e,f**). For each light curve, we can also see its fitting parameters and their errors (for very small errors we truncated the values to 0.01). Moreover, in the small subplots, we can see the peak of each light curve magnified. Furthermore, in Table 3.2 we can see the parameters that produced these specific light curves and the calculated parameters, which we used in order to decide the origin of each event.
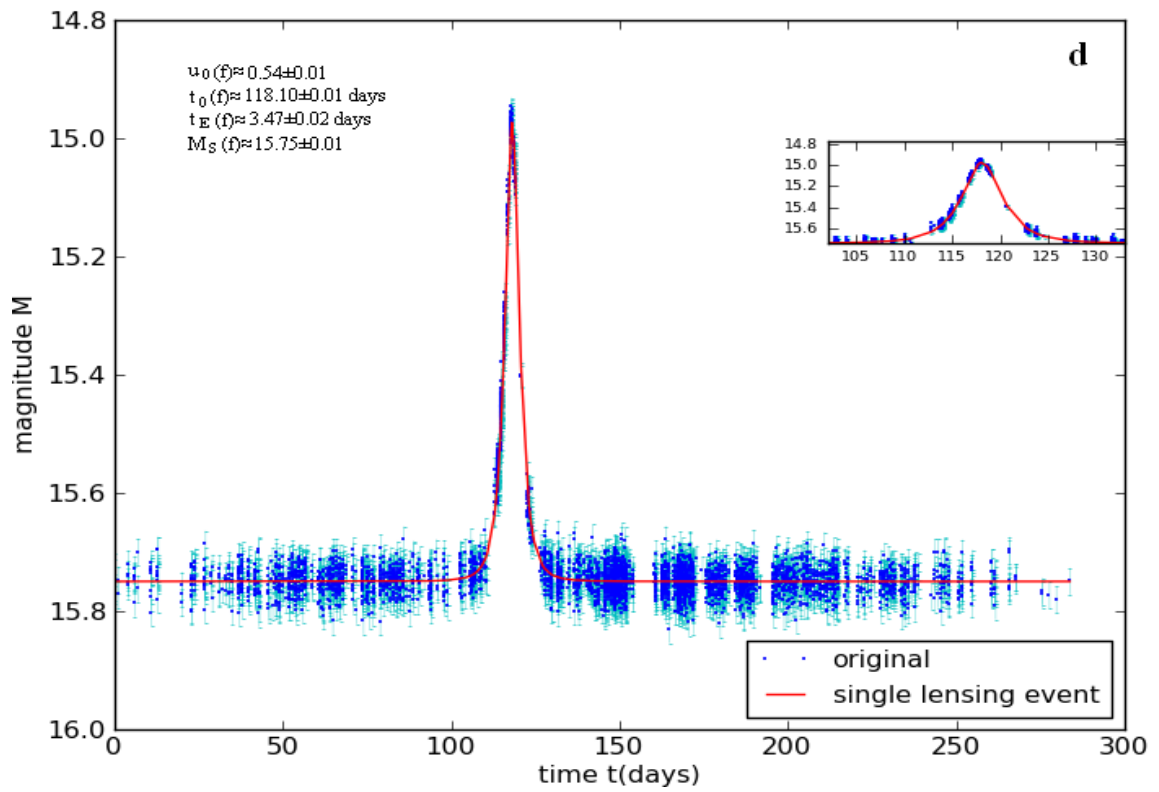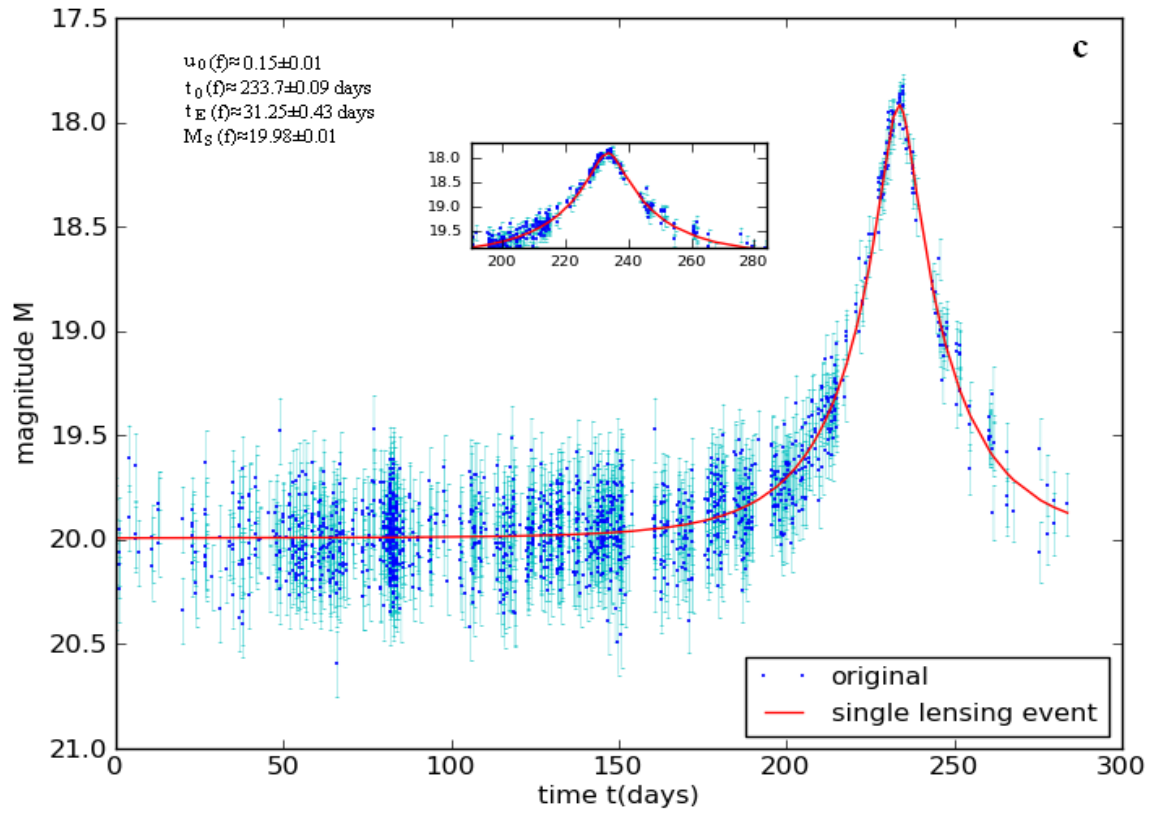
Figure 3.2 (contn.)
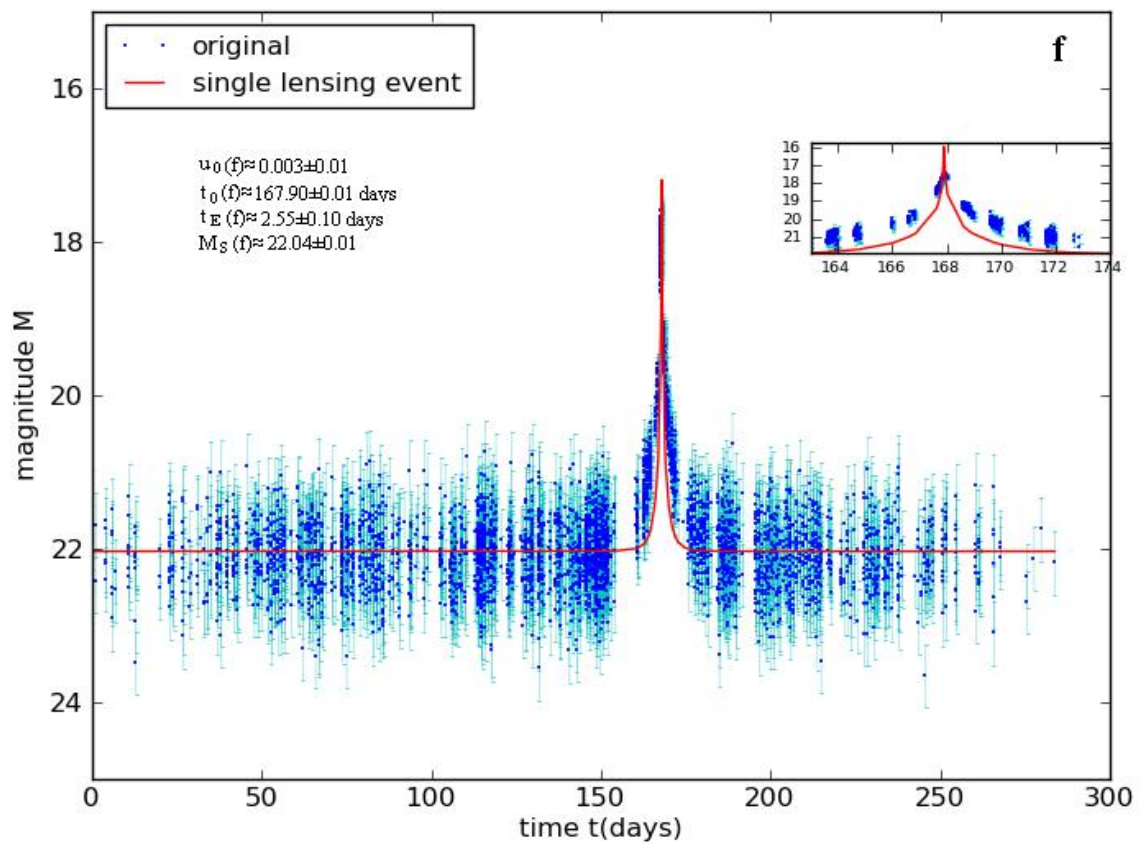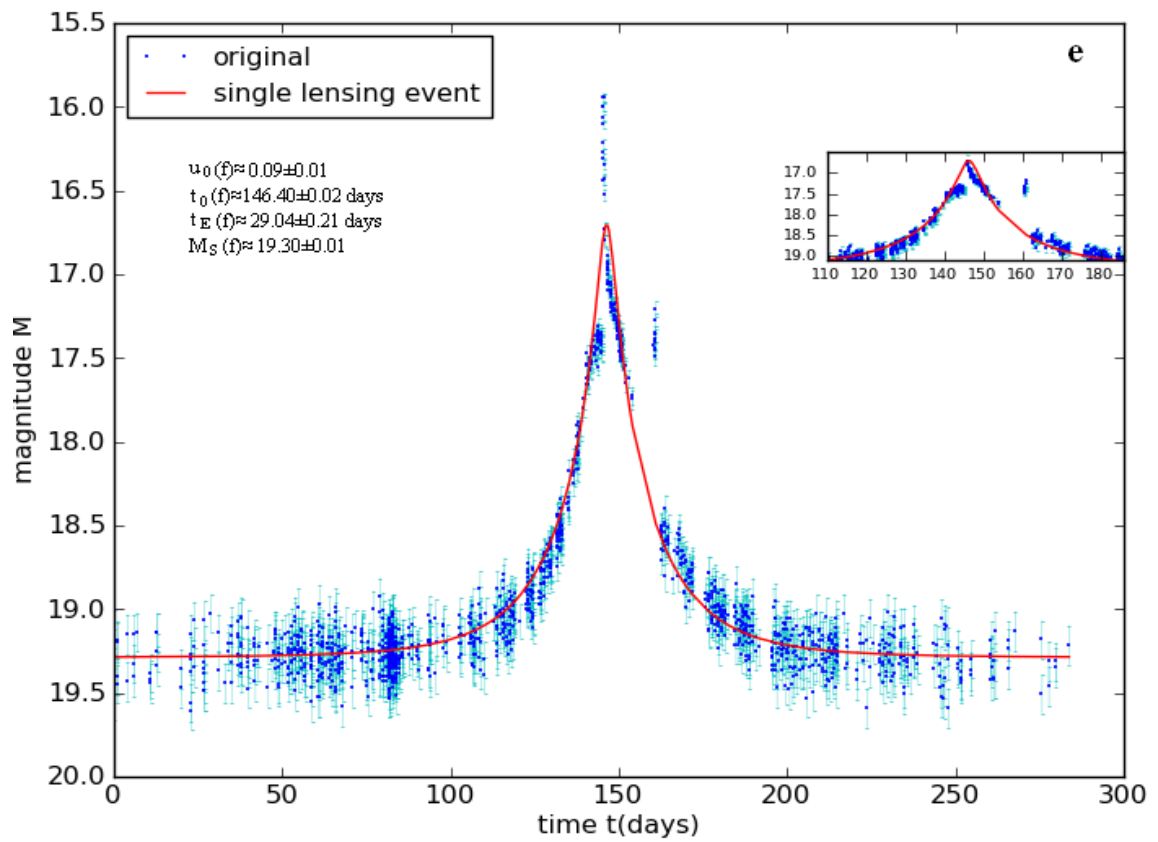
Figure 3.2 (contn.)

CHAPTER 4

PLANETARY EVENTS: FREE FLOATING OR BOUND PLANETS?

4.1 Introduction

In the previous Chapter we explained how we determined if the microlensing light curve of a binary lensing event is similar to the light curve of a free floating planet, to the light curve of a single lensing event, where the light curve seems to come from the host star or to the light curve of binary lensing event.

In the following sections we state and analyze our results.

4.2 Microlensing Light Curves That Peak Close to $t_{0(planet)}$

As mentioned before, a free floating planet-like microlensing event should be a single lensing event with fitted Einstein timescale $t_{E(f)} < 5$ and $t_{0(f)}$ close to $t_{0(planet)}$. However, we encountered cases of microlensing events with $t_{0(f)}$ close to $t_{0(planet)}$ but where $t_{E(f)}$ was longer than five days, which we defined as microlensing events where the light curve seems to come from the host star (a planet cannot be recognised reliably with such a wide peak).

In Figure 4.1 we can see the relative frequency of Einstein timescale of all the events that have $t_{0(f)}$ close to $t_{0(planet)}$ for all the planet masses, for the standard and the high cadence time sample. As can been seen, the majority of microlensing events, for which $t_{0(f)}$ is close to $t_{0(planet)}$, have Einstein timescale longer than five days thus, the majority of the events for which $t_{0(f)}$ is close to $t_{0(planet)}$ cannot be assumed to be recognised as free floating planet events.

a. Relative Frequency of Einstein timescale (tE(f))
(for all events that peak close to t0(planet) (standard cadence time sample))

b. Relative Frequency of Einstein timescale (tE(f))
(for all events that peak close to t0(planet) (high cadence time sample))
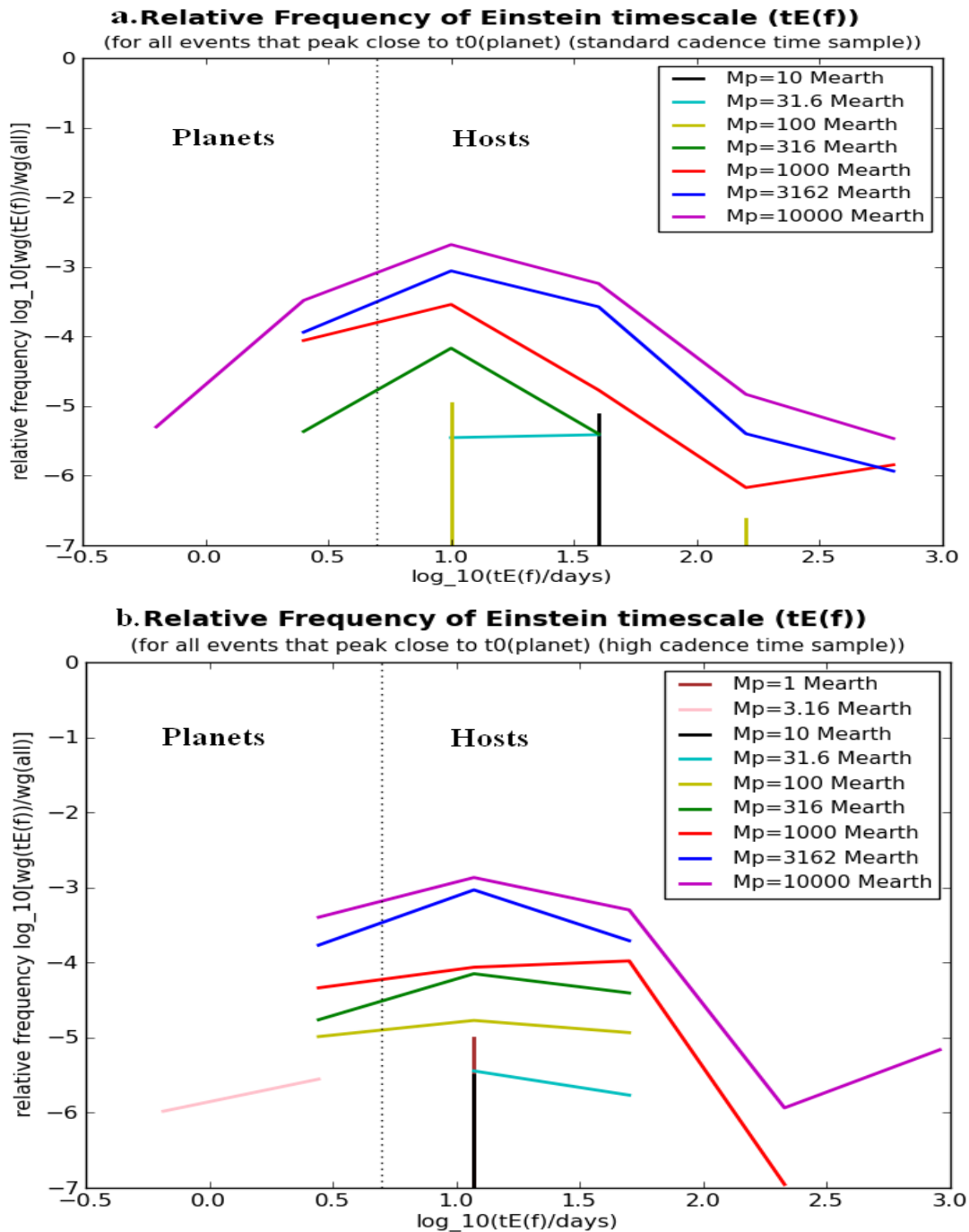
Figure 4.1 The relative frequency of Einstein timescale $t_{E(f)}$ of all single lensing events, for which $t_{0(f)}$ is close to $t_{0(planet)}$ for the standard cadence time sample (**a**) and for the high cadence time sample (**b**). The different colours indicate microlensing events that are produced, in our simulations, from different values for the mass of the planet. The dotted lines indicate the position, where $t_{E(f)}$=5 days and separate recognisable planetary from the stellar-like events. In the case of the standard time sample (**a**) for planet mass equal to 1 and 3.16 $M_{\oplus}$ we have not encountered any cases with $t_{0(f)}$ close to $t_{0(planet)}$. Some lines are truncated because the range of Einstein timescales of the events that passed our criteria (single lensing events, $t_{0(f)}$ close to $t_{0(planet)}$) at those planet masses is short.

4.3 Microlensing Event Origin

We tested the origin of 93763 simulated microlensing events, generated from the Besancon Galactic model, each one of them for 9 different planet masses, for two time samples. As we described in section 3.4, we rejected some of these events from our results for a variety of reasons and for the rest of them we determined their origin.

In Table 4.1 we can see the proportion of binary lensing events, the light curve of which, after the fitting to the light curve of a single lensing event, seems similar to that of a free floating planet, to that of a single lensing event originated from the host star or to that of a binary lensing event (Figure 4.2).

Table 4.1 The number (*No*) of free floating planet-like events, of events where the light curve seems to come from the host star and of binary lensing-like events and their relative frequency **rf** (the sum of statistical weights of events of each category (wg_{ff}, wg_{host} and wg_{bin} respectively), normalized to the statistical weight of the total of the events (wg_{all})), for each value for the mass of the planet, for the two time samples of different cadence (**a.** standard cadence time sample, **b.** high cadence time sample).

| a. Standard Cadence Time Sample						
Planet Mass ($M_\oplus$)	**Free Floating Planet-like Events**		**Events Originated From the Host Star**		**Binary Lensing-like Events**	
	No	$rf\left(\frac{wg_{ff}}{wg_{all}}\right)$	*No*	$rf\left(\frac{wg_{host}}{wg_{all}}\right)$	*No*	$rf\left(\frac{wg_{bin}}{wg_{all}}\right)$
1	0	0	74148	0.736	318	1.90×10^{-3}
3.1623	0	0	73598	0.738	336	2.30×10^{-3}
10	0	0	70935	0.718	313	2.20×10^{-3}
31.623	0	0	65282	0.686	325	2.10×10^{-3}
100	0	0	56011	0.619	306	2.40×10^{-3}
316.23	1	4.32×10^{-6}	44745	0.511	330	2.60×10^{-3}
1000	4	8.76×10^{-5}	33456	0.39	347	3.40×10^{-3}
3162.3	16	1.20×10^{-4}	23044	0.2763	506	6.00×10^{-3}
10000	34	3.40×10^{-4}	12361	0.163	817	1.10×10^{-2}
b. High Cadence Time Sample						
Planet Mass ($M_\oplus$)	**Free Floating Planet-like Events**		**Events Originated From the Host Star**		**Binary Lensing-like Events**	
	No	$rf\left(\frac{wg_{ff}}{wg_{all}}\right)$	*No*	$rf\left(\frac{wg_{host}}{wg_{all}}\right)$	*No*	$rf\left(\frac{wg_{bin}}{wg_{all}}\right)$
1	0	0	77603	0.79	391	2.50×10^{-3}
3.1623	2	3.85×10^{-6}	76349	0.79	340	2.20×10^{-3}
10	0	0	72507	0.76	328	1.80×10^{-3}
31.623	0	0	65211	0.72	353	2.20×10^{-3}
100	3	1.03×10^{-5}	54262	0.63	304	2.20×10^{-3}
316.23	4	7.54×10^{-6}	42122	0.51	349	3.00×10^{-3}
1000	3	1.90×10^{-5}	30641	0.38	423	4.00×10^{-3}
3162.3	10	1.60×10^{-4}	20582	0.26	577	6.50×10^{-3}
10000	34	3.70×10^{-4}	10692	0.15	880	1.14×10^{-2}
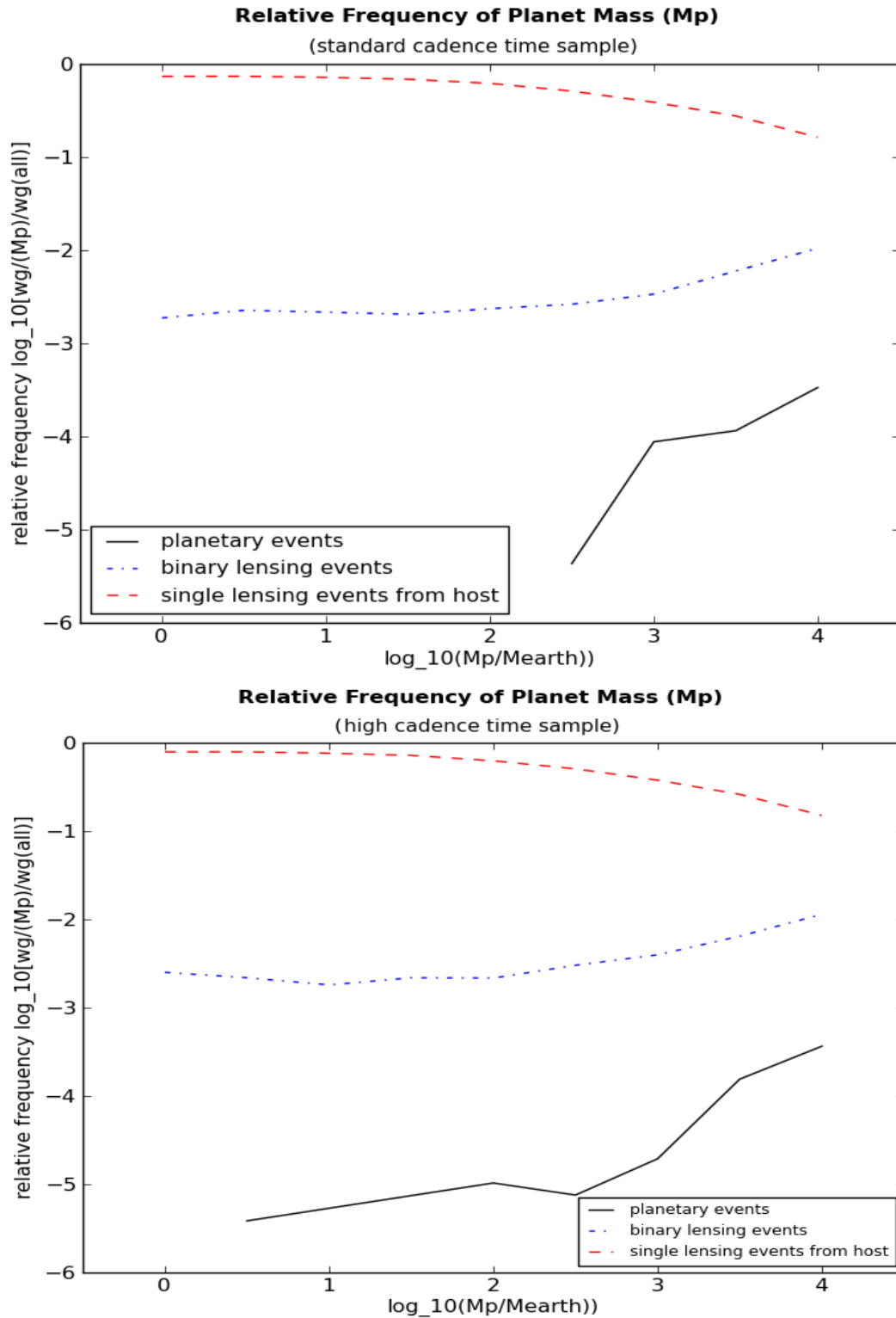
Figure 4.2   The relative frequency $\log\_10[wg/(M_p)/wg(all)]$ of free-floating planet like events (planetary events), binary lensing events and single lensing events where the light curve seems to come from the host star (single lensing events from host), for each planet mass, for the standard (**a**) and for the high (**b**) cadence time sample.

As it can been seen in the Figure 4.2, the proportion of free floating planet-like events is extremely small or even zero as it was expected for small values of planet mass, especially for the standard cadence time sample, since the duration of a microlensing event of an object of small mass is extremely short (some hours) and thus, the frequency of observations, even for the high cadence time sample, is not high enough for its detection. For the same reason, we encounter slightly more free floating planet-like events in the cases of small planet mass, for the high cadence time sample.

4.4 Microlensing Event Parameters

In the previous section we determined the proportion of microlensing events of each kind (free floating planet-like events, single lensing events where the light curve comes from the host star and binary lensing-like events), which resulted from our simulations. In this section, we will discuss about some of the parameters of these events.

Einstein Timescale ($t_{E(f)}$)

As mentioned in Section 2.1, the Einstein timescale (t_E) defines the duration of a microlensing event and depends on the transverse velocity (v_t), the distance of the source (D_S), the distance of the lens (D_L) and the mass of the lens (M_L). As a consequence, in our simulations, the fitting parameter for the Einstein timescale ($t_{E(f)}$) is the parameter that gave us information about the length of a microlensing event and thus, the mass of the lensing object and the origin of the event.

In Figure 4.3 we can see the calculated rate-weighted relative frequency of Einstein timescale $t_{E(f)}$ of the events of each kind (free floating planet-like, binary-like and host star-like events), for each planet mass, for the standard (**a**) and for the high (**b**) cadence time sample.
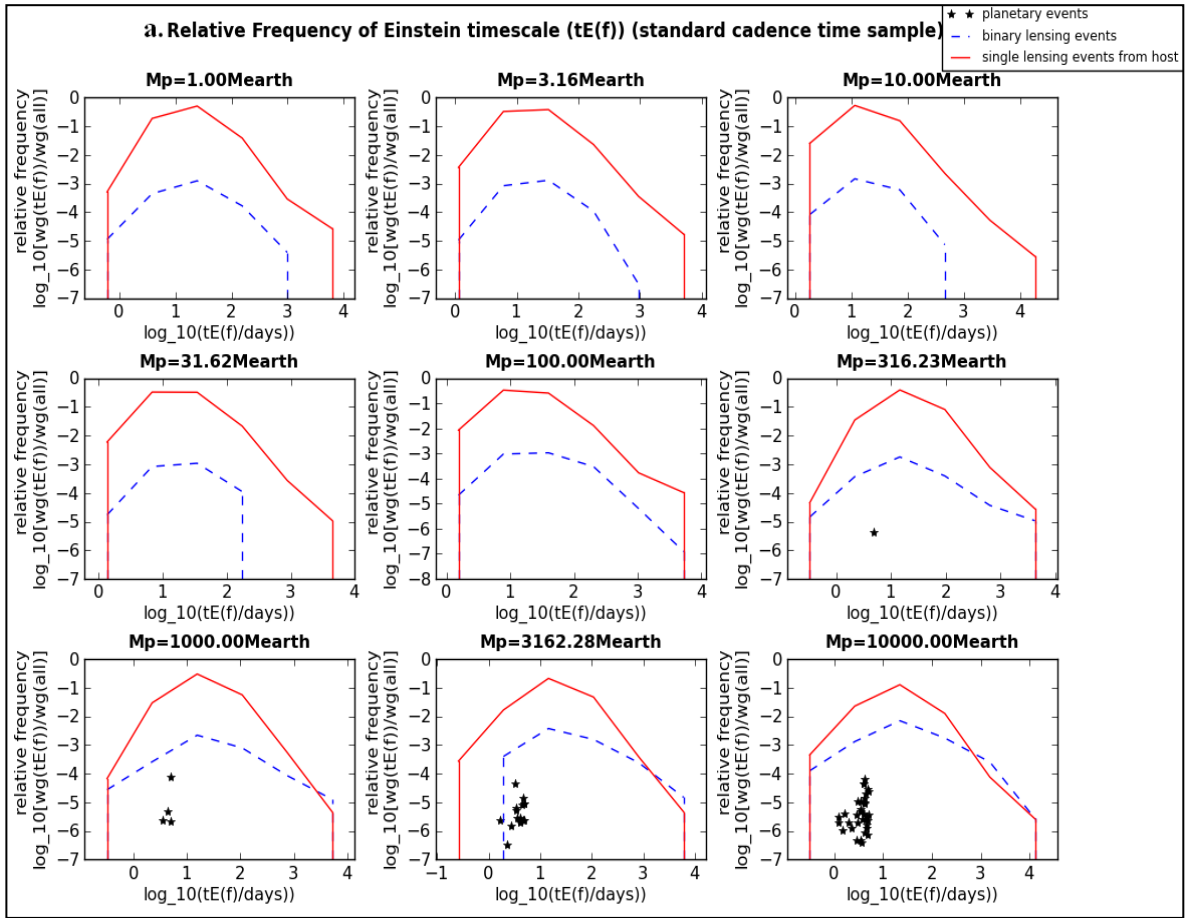
Figure 4.3 The relative frequency of Einstein timescale $t_{E(f)}$, for each planet mass-value, for the standard (**a**) and for the high (**b**) cadence time sample. The star points indicate the relative frequency of Einstein timescale for each free floating planet-like microlensing event from our simulation, the blue dashed lines indicate the relative frequency of Einstein timescale for the binary-like microlensing events and the red solid lines indicate the relative frequency of Einstein timescale for the single lensing events, the light curve of which seems to come from the host star.
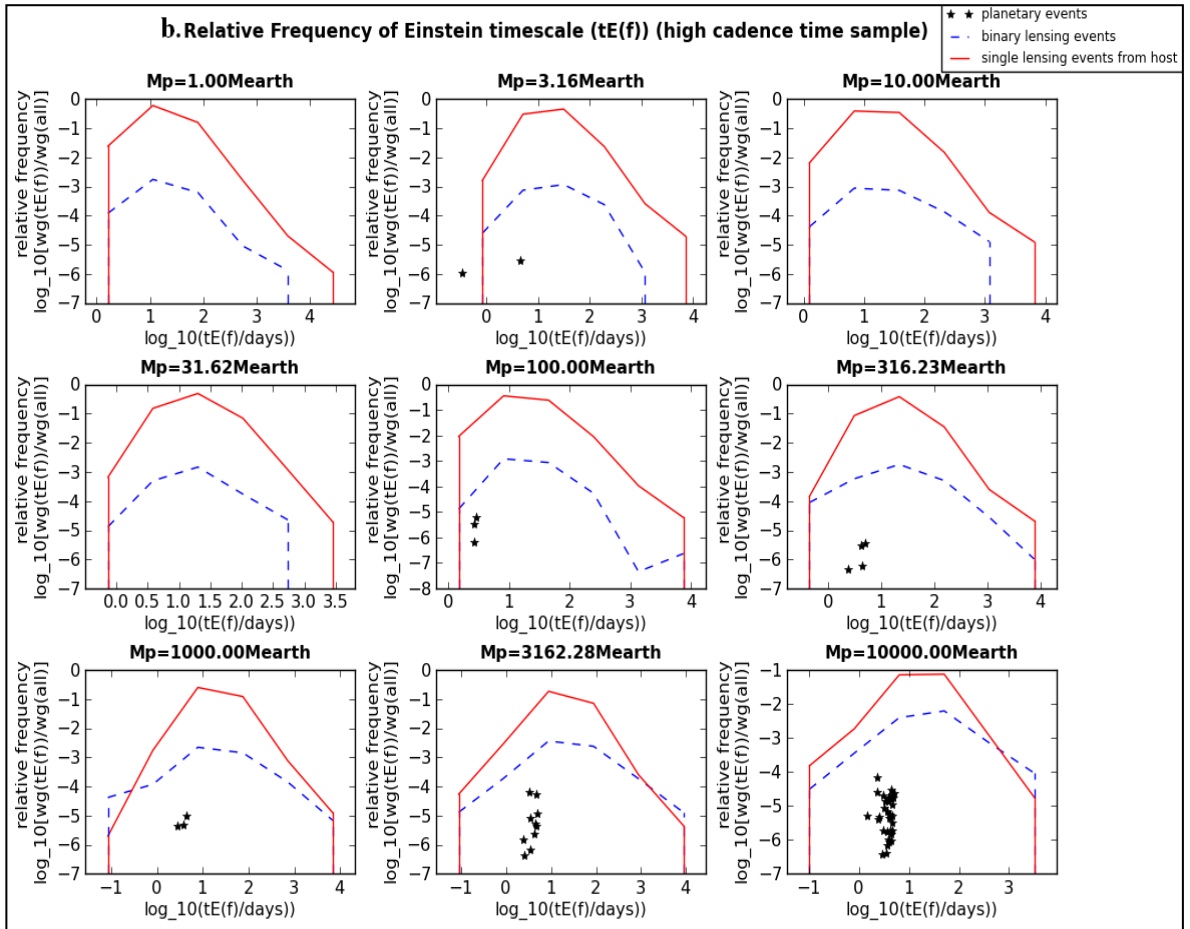
Figure 4.3 (contn.)

By the construction of our selection criteria (Section 3.5) we know that all the free floating planet-like microlensing events have an Einstein timescale less than five days but furthermore, as it can be seen in the Figure 4.3 the majority of them have an Einstein timescale more than two days, which is the value that Sumi et al. (2011) assumed as the upper limit for the Einstein timescale of the free-floating planet microlensing events (Figure 1.6).

Moreover, as it is obvious from the Figure 4.3, the majority of the binary-like and the host star-like microlensing events have an Einstein timescale from 10 to 100 days (we do not encounter many high or short Einstein timescales), which means that in the Besancon input catalogue of stars that we used for our simulations there are only few stars with high transverse velocity (when the transverse velocity is high, the calculated Einstein timescale is short (Equation 2.15)) and additionally only few massive stars (when the mass

of the lens (in our case the mass of the lens star) is big, the calculated Einstein timescale is long (Equations 2.11, 2.15)).

Sky-Projected Separation (*s*)

As we have shown in Section 1.2, although that the majority of the detected bound exoplanets have a semi-major axis that ranges from 0.01 to 10 AU there are some of them in a much more distant orbit from their host. In the specific cases of the exoplanets detected with the method of gravitational microlensing the semi-major axis is typically larger than for the radial velocity or transit methods, since it ranges from 0.66 to 8.3 AU (Schneider 2012).

In our simulations we used logarithmically random values of host-planet sky-projected separation (a lower limit to the true host-planet orbital separation) from 0.1 to 100 AU (for projected separations longer than 100 AU we can not be certain that the planet is bound) in order to examine if long separations can result in a light curve that cannot be differentiated from the light curve of a free floating planet.

Consequently, we test if the value of the sky-projected separation can affect our results. In Figure 4.4 we can see the relative frequency of sky-projected separation for events of each kind (free floating planet-like, binary-like and host star-like events), for all planet mass values that produced free floating planet-like events in our simulations, for the standard (**a**) and for the high (**b**) cadence time sample.
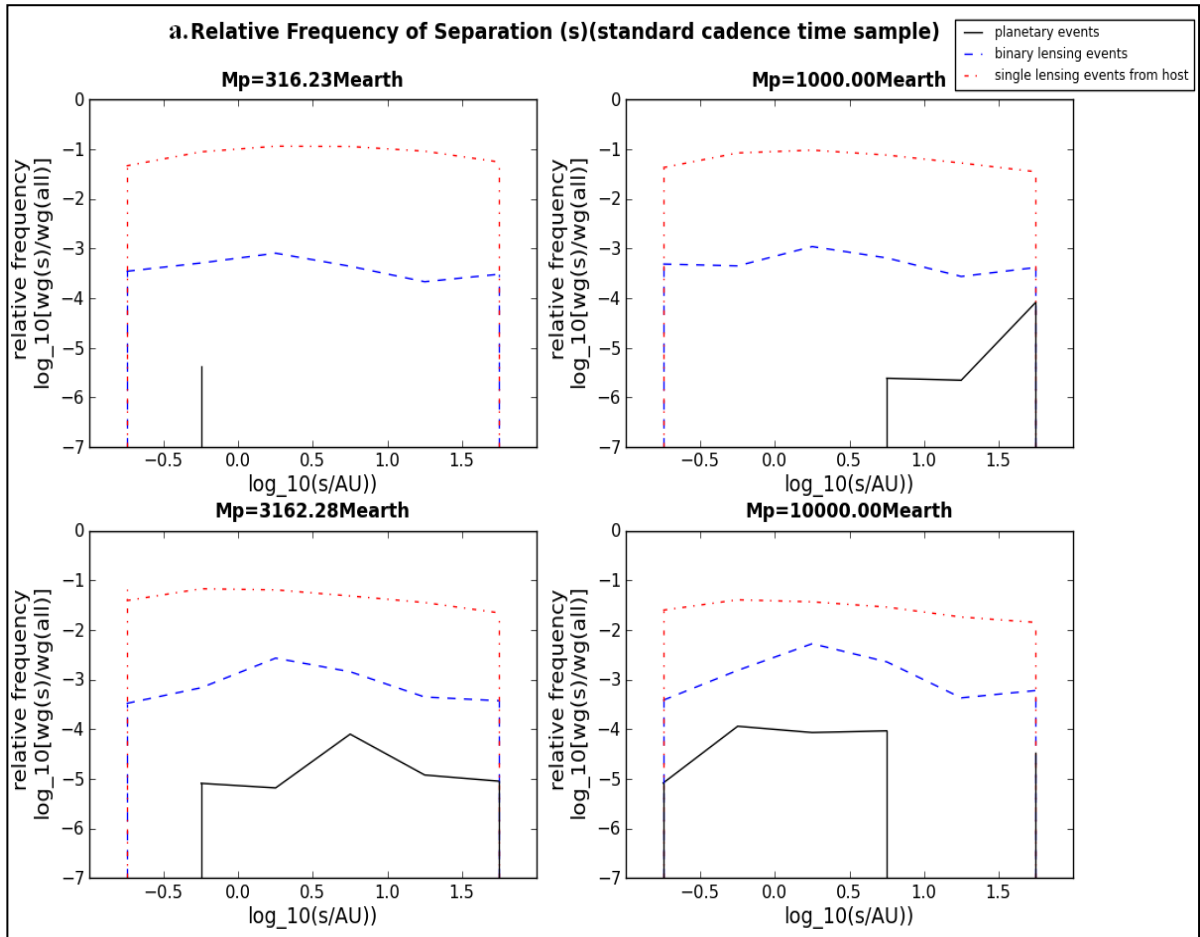
Figure 4.4 The relative frequency of host-planet sky-projected separation *s*, for each planet mass-value that produced free floating planet-like events, for the standard (**a**) and for the high (**b**) cadence time sample. The solid black lines indicate the relative frequency of sky-projected separation for the free floating planet-like microlensing events, the blue dashed lines indicate the relative frequency of sky-projected separation for the binary-like microlensing events and the red dashed-dotted lines indicate the relative frequency of sky-projected separation for the single lensing events, the light curve of which seems to come from the host star.
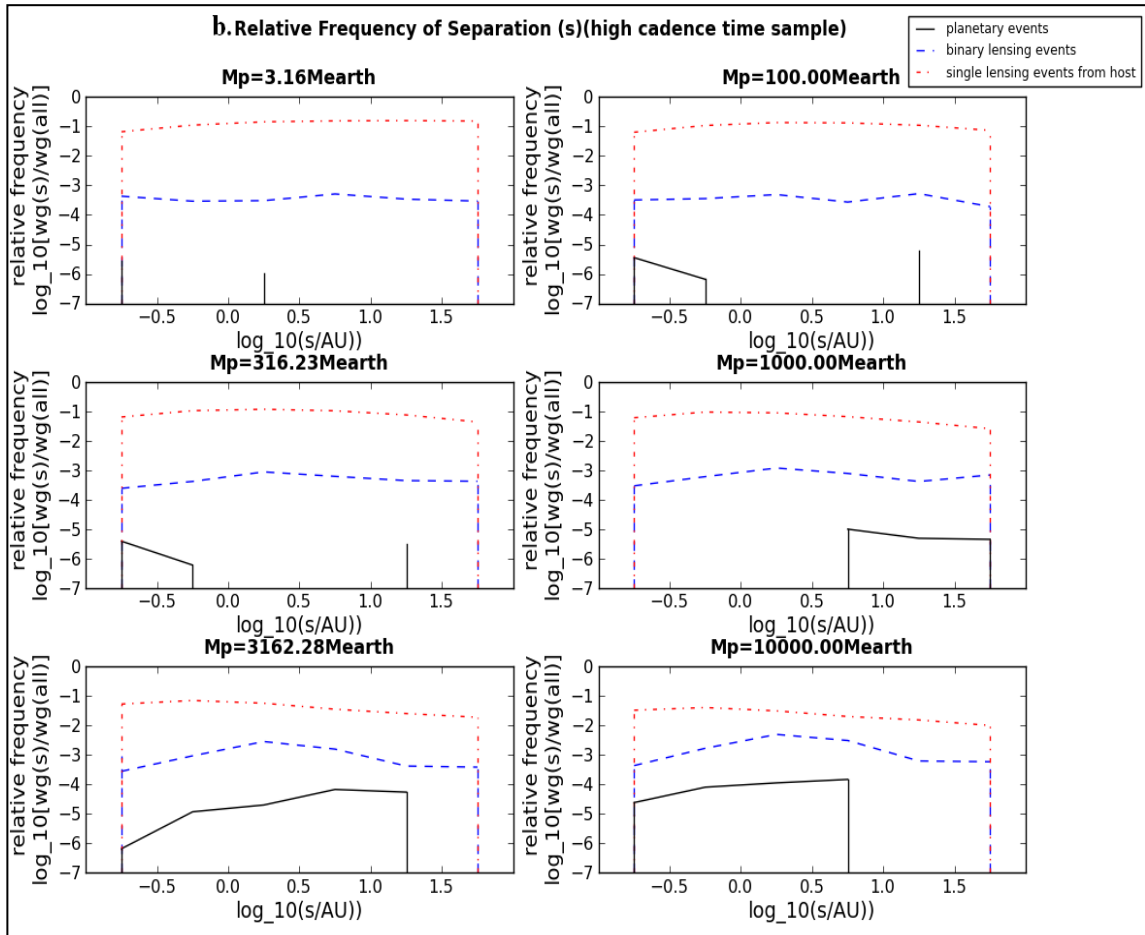
Figure 4.4 (contn.)

As it can been seen in the Figure 4.4, the host-planet sky-projected separation for the free floating planet-like events ranges between all the possible values and thus, it can be assumed that there are no values of separation (at least in the range from 0.01 to 100 AU) that result in higher frequency of occurrence of free floating planet-like events. However, given the relatively small number of simulated events, which pass our criteria as free floating–like signals, it is possible that we are unable to resolve underlying trends with separation without undertaking a larger scale simulation.

Furthermore, we can see that the sky-projected separation for the host-like events reflects the input distribution and thus, all values of separation can result in this kind of events with the same frequency. The sky-projected separation for the binary-like events has a small deviation from the input distribution but this can be considered as a result of the relative small sample of these events.

4.5 Comparison with Sumi et al. (2011)

As mentioned in Section 1.4, Sumi et al. (2011) discovered a population of free floating planets with the method of gravitational microlensing. To specify, Sumi et al. (2011) analyzed the data from 2006-2007 MOA-II, where about a thousand microlensing events were found. Ten of these events, that have an Einstein timescale less than two days, have been recognized as free floating planet events (Figure 1.11).

In the section 4.3 we calculated the relative frequency of free floating planet-like microlensing events, from a sample of 93763 generated binary microlensing events, for nine planet masses and for two time samples.

In this section we will show what fraction of the Sumi et al. (2011) free floating planet events could be in reality binary lensing events. For this reason and since in our simulations we set as an upper limit for the free floating planet-like events $t_E < 5$ days (and not the two days as Sumi et al. (2011) did for the discovered free floating planets), we need to calculate the relative frequency $\left(rf(wg_{ff(tE(f)<2)}/wg_{all})\right)$ of the free floating planet-like events of our simulations, which have an Einstein timescale less than two days $(t_{E(f)} < 2\ days)$.

Furthermore, in order to find what fraction of the free floating planet events discovered by Sumi et al. (2011) are in reality binary lensing events, we multiply the relative frequency $\left(rf(wg_{ff}/wg_{all})\right)$ of all free floating planet-like events (assuming a higher limit for the Einstein timescale of free floating planet events than Sumi et al. (2011) did) (Table 4.1) and the relative frequency $\left(rf(wg_{ff(tE(f)<2)}/wg_{all})\right)$ of free floating planet-like events with Einstein timescale less than two days $(t_{E(f)} < 2\ days)$, which we found in our simulations, by 1000, which is the total number of microlensing events analysed in the sample of Sumi et al. (2011).

In Table 4.2, we can see the relative frequency $\left(\boldsymbol{rf(wg_{ff(tE(f)<2)}/wg_{all})}\right)$ of free floating planet-like events that resulted from our simulations, for which the Einstein timescale is less than two days $(t_{E(f)} < 2\ days)$ and the fraction (N_P **(per 1000 events)**) of microlensing events from the sample of Sumi et al. (2011), for which, according to our simulations, cannot be clear if the origin is a free floating or a bound planet, for both upper

limits for the Einstein timescale of free floating planet-like events ($t_{E(f)} < 5$ days and $t_{E(f)} < 2$ days), for the nine planet masses, for both, simulated, time samples (Figure 4.5).
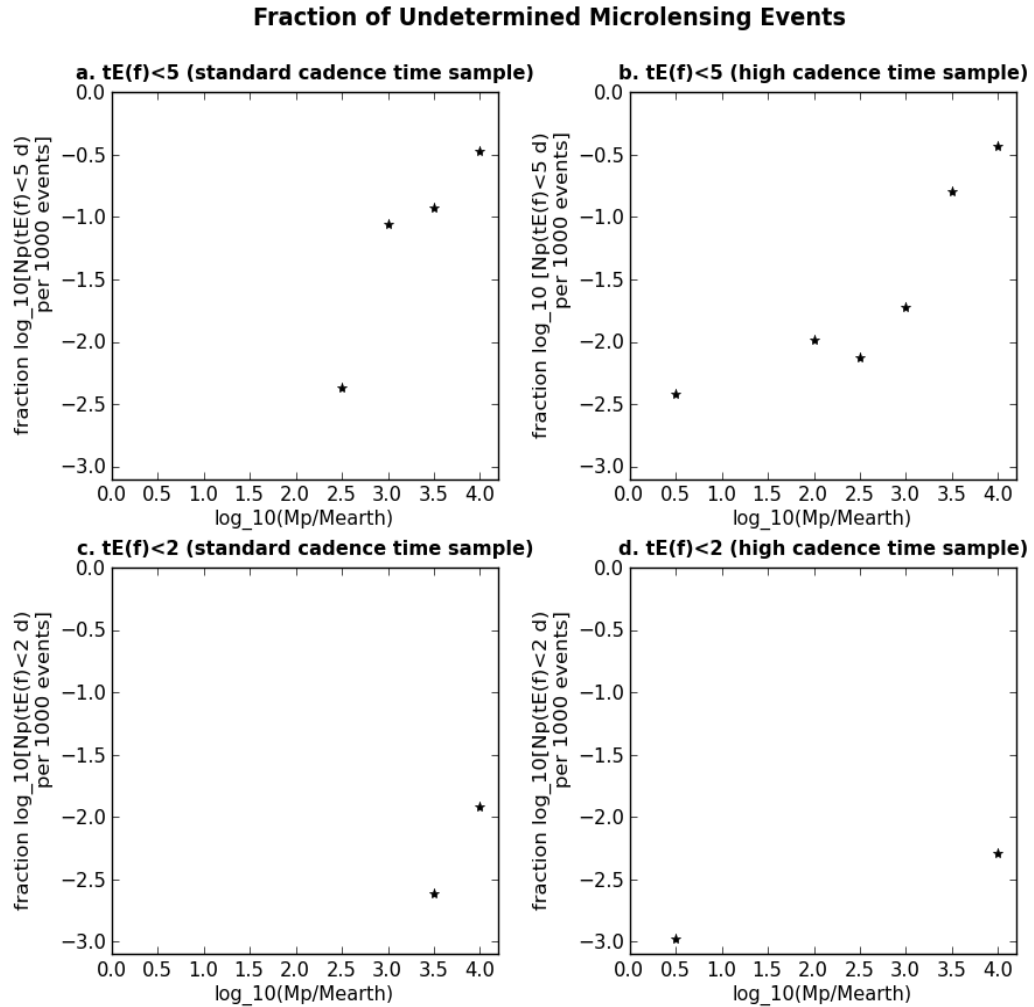
Figure 4.5 The fraction (N_P (per 1000 events)) of the undetermined, according to our simulations, microlensing events from the sample of Sumi et al. (2011), for two upper limits for the Einstein timescale of free floating planet-like events ($t_{E(f)} < 5$ days (**a,b**) and $t_{E(f)} < 2$ days (**c,d**)), for each planet mass-value, for the standard (**a,c**) and for the high (**b,d**) cadence time sample.

Table 4.2 The relative frequency $\left(rf\left(wg_{ff(tE(f)<2)}/wg_{all}\right)\right)$ of all free floating planet-like events of our simulations that have an Einstein timescale less than two days ($t_{E(f)} < 2\ days$) and the fraction (N_P (per 1000 events)) of microlensing events from the sample of Sumi et al. (2011), for which, according to our simulations, we cannot determine if the origin is a free floating or a bound planet, for both upper limits for the Einstein timescale of free floating planet-like events ($t_{E(f)} < 5$ days and $t_{E(f)} < 2$ days), for the nine planet mass-values, for the standard (**a**) and for the high (**b**) cadence time sample.

a. Standard Cadence Time Sample			
$M_p(M_\oplus)$	rf $\left(\dfrac{wg_{ff(tE(f)<2)}}{wg_{all}}\right)$	$N_{P(tE(f)\,<\,5\ days)}$ (per 1000 events) $\left(rf\left(\dfrac{wg_{ff}}{wg_{all}}\right) \times 1000\right)$	$N_{P(tE(f)\,<\,2\ days)}$ (per 1000 events) $\left(rf\left(\dfrac{wg_{ff(tE(f)<2)}}{wg_{all}}\right) \times 1000\right)$
1	0	0	0
3.1623	0	0	0
10	0	0	0
31.623	0	0	0
100	0	0	0
316.23	0	4.32×10^{-3}	0
1000	0	8.76×10^{-2}	0
3162.3	2.43×10^{-6}	1.20×10^{-1}	2.43×10^{-3}
10000	1.22×10^{-5}	3.40×10^{-1}	1.22×10^{-2}
b. High Cadence Time Sample			
$M_p(M_\oplus)$	rf $\left(\dfrac{wg_{ff(tE(f)<2)}}{wg_{all}}\right)$	$N_{P(tE(f)\,<\,5\ days)}$ (per 1000 events) $\left(rf\left(\dfrac{wg_{ff}}{wg_{all}}\right) \times 1000\right)$	$N_{P(tE(f)\,<\,2\ days)}$ (per 1000 events) $\left(rf\left(\dfrac{wg_{ff(tE(f)<2)}}{wg_{all}}\right) \times 1000\right)$
1	0	0	0
3.1623	1.05×10^{-6}	3.85×10^{-3}	1.05×10^{-3}
10	0	0	0
31.623	0	0	0
100	0	1.03×10^{-2}	0
316.23	0	7.54×10^{-3}	0
1000	0	1.90×10^{-2}	0
3162.3	0	1.60×10^{-1}	0
10000	5.18×10^{-6}	3.70×10^{-1}	5.18×10^{-3}

As mentioned before, Sumi et al. (2011) assumed that the free floating planet events should have an Einstein timescale less than two days and according to this assumption they detected ten free floating planet events.

As it can been seen in the Figure 4.5 (**c**,**d**), there is only a very small fraction (much less than the 10 that Sumi et al. (2011) discovered) for which the origin is actually due to a bound planet for both time samples. Even if we assume that the upper limit for the Einstein timescale is the 5 days ($t_E < 5$ days) (Figure 4.5 (**a**,**b**),) the fraction of the undetermined microlensing events would be still very small (much less than 10).

As a result, we can conclude that the origin of the free floating planet events that Sumi et al. (2011) discovered is indeed consistent with unbound planets or bound planets with sky-projected separations from their host longer than 100 AU.

CHAPTER 5

CONCLUSIONS AND FUTURE WORK

Since the first detections of extrasolar planets in 1992, around a pulsar (Wolszczan et al. 1992; Wolszczan 1994) and in 1995, around a star (Mayor et al. 1995), hundreds of exoplanets have been discovered. The progress of technology developed the methods used for the detection of exoplanets and as a result more and more exoplanets are detected with various masses down to the mass of Earth or smaller and various orbital properties.

The method of gravitational microlensing is considered to be very sensitive to the detection of faint objects and thus, it can be applicable to the detection of free floating (unbound) planets (Bennett et al. 2007). Around one year ago, Sumi et al. (2011) claimed the discovery of a Galactic free floating planet population with the method of gravitational microlensing. In this work, we tested if this discovered free floating planet population could be in reality bound planets that produce microlensing light curves very similar to that of free floating planets.

For this reason, we simulated binary microlensing events (which afterwards we fitted to a single lensing event), produced by different parameters for the source star, the lens star and the planet, in order to determine if there is any possibility for a binary microlensing event to produce a microlensing light curve, which cannot be differentiated from the light curve of a free floating planet.

To specify, we simulated real time observations of MOA (data came from: MOA[7]) and got the input parameters for the source and the lens star from synthetic microlensing simulations (Kerins et al. 2009) generated from the Besancon Galactic model (Robin et al. 2003; Marshall et al. 2006). We used these synthetic parameters to generate artificial binary lens light curves for a range of planet masses (1 to 10000 $M_\oplus$) and host-planet sky-projected separations (0.1 to 100 AU). We used standard and high cadence epoch distributions from selected MOA events to generate realistic light curve photometry and then we fitted the light curves with a single lens model. By applying cuts to the timescale, goodness of fit and the epoch of the peak we defined samples which showed clear binarity, evidence of an ordinary host-like single-lens signal and evidence of a planet-like free floating signal.

---

[7] https://it019909.massey.ac.nz/moa/alert/, [date of access: 14th of July 2012].

Our results have shown that the possibility for a binary microlensing event to be confused as a free floating planet event is extremely small, at least for host-planet sky-projected separations from 0.1 to 100 AU. Future work should test this possibility for separations longer than 100 AU. Furthermore, larger scale simulations may be needed to investigate how the frequency of free floating-like binary light curves is sensitive to host separation.

Finally, in regard to the free floating planet population that Sumi et al. (2011) discovered, it is concluded that these planets are actually unbound or at least they do not have any host at sky-projected separations equal or less than 100 AU.

References

Alibert Y., Mordasini C., Benz W. 2011, 2011A&A...526A..63A

Alibert Y., Mordasini C., Benz W., Winisdoerffer C. 2005, 2005A&A...434..343A

Baraffe I., Chabrier G., Barman T. S., Allard F., Hauschildt P. H. 2003, 2003A&A...402..701B

Barry R., Kruk J., Anderson J., Beaulieu J.-P., Bennett D. P., Catanzarite J., Cheng E., Gaudi S., Gehrels N., Kane S., Lunine J., Sumi T., Tanner A., Traub W. 2011, 2011SPIE.8151E..19B

Batalha N. M., Kepler Team 2012, 2012AAS...22030601B

Beaulieu J. P., Bennett D. P., Batista V., Cassan A., Kubas D., Fouqué; P., Kerrins E., Mao S., Miralda-Escudé; J., Wambsganss J., Gaudi B. S., Gould A., Dong S. 2010, 2010ASPC..430..266B

Beaulieu J.-P., et al. 2006, 2006Natur.439..437B

Beckwith S. V. W., Sargent A. I. 1996, 1996Natur.383..139B

Bennett D. P., et al. 2008, 2008ApJ...684..663B

Bennett D. P., Rhie S. H. 1996, 1996ApJ...472..660B

Bodenheimer P., Laughlin G., Lin D. N. C. 2003, 2003ApJ...592..555B

Bodenheimer P., Lin D. N. C., Mardling R. A. 2001, 2001ApJ...548..466B

Bodenheimer P., Pollack J. B. 1986, 1986Icar...67..391B

Bond I. A. 2012, 2012NewAR..56...25B

Bond I. A., et al. 2004, 2004ApJ...606L.155B

Borucki W. J., et al. 2010, 2010Sci...327..977B

Boss A. P., Weinberger A. J., Anglada-Escudé; G., Thompson I. B., Burley G., Birk C., Pravdo S. H., Shaklan S. B., Gatewood G. D., Majewski S. R., Patterson R. J. 2009, 2009PASP..121.1218B

Boss A. P. 1997, 1997Sci...276.1836B

Burrows A., Hubeny I., Budaj J., Hubbard W. B. 2007, 2007ApJ...661..502B

Butler R. P., Marcy G. W. 1996, 1996ApJ...464L.153B

Butters O. W., West R. G., Anderson D. R., Collier Cameron A., Clarkson W. I., Enoch B., Haswell C. A., Hellier C., Horne K., Joshi Y., Kane S. R., Lister T. A., Maxted P. F.L., Parley N., Pollacco D., Smalley B., Street R. A., Todd I., Wheatley P. J., Wilson D. M. 2010, 2010A&A...520L..10B

Caballero J. A., Béjar V. J. S., Rebolo R., Eislöffel J., Zapatero Osorio M. R., Mundt R., Barrado Y Navascués D., Bihain G., Bailer-Jones C. A. L., Forveille T., Martín E. L. 2007, 2007A&A...470..903C

Campbell B., Walker G. A. H., Yang S. 1988, 1988ApJ...331..902C

Carpenter J. M., Wolf S., Schreyer K., Launhardt R., Henning T. 2005, 2005AJ....129.1049C

Cassan A., et al. 2012, 2012Natur.481..167C

Charbonneau D., Brown T. M., Burrows A., Laughlin G. 2007, 2007prpl.conf..701C

Cieza L., Padgett D. L., Stapelfeldt K. R., Augereau J.-C., Harvey P., Evans N. J., II, Merín B., Koerner D., Sargent A., van Dishoeck E. F., Allen L., Blake G., Brooke T., Chapman N., Huard T., Lai S.-P., Mundy L., Myers P. C., Spiesman W., Wahhaj Z. 2007, 2007ApJ...667..308C

Copernicus N. 1543, 1543droc.book.....C

Crane J. D., Shectman S. A., Butler R. P. 2006, 2006SPIE.6269E..96C

Cui X., Yuan X., Gong X. 2008, 2008SPIE.7012E..83C

Cumming A., Marcy G. W., Butler R. P. 1999, 1999ApJ...526..890C

del Burgo C., Allende Prieto C., Peacocke T. 2010, 2010JInst...5.1006D

Deming D., Harrington J., Seager S., Richardson L. J. 2006, 2006ApJ...644..560D

Doyle L. R., et al. 2011, 2011Sci...333.1602D

Galilei G. 1989, 1989QB41.G173......

Gaudi B. S., et al. 2008, 2008Sci...319..927G

Gehman C. S., Adams F. C., Laughlin G. 1996, 1996PASP..108.1018G

Goldreich P., Tremaine S. 1980, 1980ApJ...241..425G

Gonzalez G., Laws C., Tyagi S., Reddy B. E. 2001, 2001AJ....121..432G

Gonzalez G. 1998, 1998A&A...334..221G

Gonzalez G. 1997, 1997MNRAS.285..403G

Gould A., et al. 2010, 2010ApJ...720.1073G

Gould A. 1994, 1994ApJ...421L..71G

Gould A. 1992, 1992ApJ...392..442G

Haisch K. E., Jr., Lada E. A., Lada C. J. 2001, 2001ApJ...553L.153H

Han C. 2006, 2006ApJ...644.1232H

Hatzes A. P., Cochran W. D., Endl M., McArthur B., Paulson D. B., Walker G. A. H., Campbell B., Yang S. 2003, 2003ApJ...599.1383H

Holman M. J., Murray N. W. 2005, 2005Sci...307.1288H

Huygens C., Rabus P., Snelders H. A. M. 1989, 1989QB41.H8512.....

Ida S., Lin D. N. C. 2004, 2004ApJ...616..567I

Ikoma M., Nakazawa K., Emori H. 2000, 2000ApJ...537.1013I

Jaroszynski M., Paczynski B. 2002, 2002AcA....52..361J

Jones B. W., Sleep P. N., Chambers J. E. 2001, 2001A&A...366..254J

Kasting J. F., Whitmire D. P., Reynolds R. T. 1993, 1993Icar..101..108K

Kerins E., Robin A. C., Marshall D. J. 2009, 2009MNRAS.396.1202K

Kim S.-L., Park B.-G., Lee C.-U., Yuk I.-S., Han C., O'Brien T., Gould A., Lee J. W., Kim D.-J. 2010, 2010SPIE.7733E.107K

Kirk G. S., Raven J. E., Schofield M., 1962. *The Presocratic Philosophers.* The University Press, Cambridge, England. *Selections from Early Greek Philosophy* by Milton C. Nahm. pp127, 418.

Konacki M., Torres G., Jha S., Sasselov D. D. 2003, 2003Natur.421..507K

Lanza A. F., De Martino C., Rodonò M. 2008, 2008NewA...13...77L

Lardièere O., Schneider J. 2008, 2008poii.conf..371L

Laughlin G., Steinacker A., Adams F. C. 2004, 2004ApJ...608..489L

Laughlin G. 2000, 2000ApJ...545.1064L

Lecavelier des Etangs A., Vidal-Madjar A., McConnell J. C., Hébrard G. 2004, 2004A&A...418L...1L

Lin D. N. C., Bodenheimer P., Richardson D. C. 1996, 1996Natur.380..606L

Lin D. N. C., Papaloizou J. 1985, 1985prpl.conf..981L

Lissauer J. J. 1999, 1999Natur.398..659L

Lissauer J. J. 1993, 1993ARA&A..31..129L

Mao S. 2008, 2008mmc..confE...2M

Mao S., Paczynski B. 1991, 1991ApJ...374L..37M

Marcy G. W., Butler R. P. 1998, 1998ARA&A..36...57M

Marcy G. W., Butler R. P. 1996, 1996ApJ...464L.147M

Marois C., Zuckerman B., Konopacky Q. M., Macintosh B., Barman T. 2010, 2010Natur.468.1080M

Marshall D. J., Robin A. C., Reylé; C., Schultheis M., Picaud S. 2006, 2006A&A...453..635M

Mayor M., Marmier M., Lovis C., Udry S., Ségransan D., Pepe F., Benz W., Bertaux J. -L., Bouchy F., Dumusque X., Lo Curto G., Mordasini C., Queloz D., Santos N. C. 2011, 2011arXiv1109.2497M

Mayor M., Queloz D. 1995, 1995Natur.378..355M

Méndez A., Candelaria J. F., 2012, *The Habitable Exoplanet Catalog 2012*, Planetary Habitability Laboratory@UPR Arecibo (phl.upr.edu); [online]. Available at: <http://phl.upr.edu/projects/habitable-exoplanets-catalog/> [date of access: 20th of August 2012].

Miralda-Escudé J. 1996, 1996ApJ...470L.113M

Mizuno H. 1980, 1980PThPh..64..544M

Murray N., Hansen B., Holman M., Tremaine S. 1998, 1998Sci...279...69M

Murray-Clay R. A., Chiang E. I., Murray N. 2009, 2009ApJ...693...23M

Naef D., Mayor M., Beuzit J. L., Perrier C., Queloz D., Sivan J. P., Udry S. 2004, 2004A&A...414..351N

Owen T. 1980, 1980ASSL...83..177O

Paczynski B. 1996, 1996ARA&A..34..419P

Peña Ramírez K., Béjar V. J. S., Zapatero Osorio M. R., Petr-Gotzens M. G., Martín E. L. 2012, 2012ApJ...754...30P

Perryman M. A. C. 2000, 2000RPPh...63.1209P

Pollacco D., et al. 2008, 2008MNRAS.385.1576P

Pollack J. B., Hubickyj O., Bodenheimer P., Lissauer J. J., Podolak M., Greenzweig Y. 1996, 1996Icar..124...62P

Pont F., Melo C. H. F., Bouchy F., Udry S., Queloz D., Mayor M., Santos N. C. 2005, 2005A&A...433L..21P

Quanz S. P., Goldman B., Henning T., Brandner W., Burrows A., Hofstetter L. W. 2010, 2010ApJ...708..770Q

Queloz D. 2006, 2006Natur.439..400Q

Rasio F. A., Ford E. B. 1996, 1996Sci...274..954R

Reiners A., Bean J. L., Huber K. F., Dreizler S., Seifahrt A., Czesla S. 2010, 2010ApJ...710..432R

Robin A. C., Reylé; C., Derrière S., Picaud S. 2003, 2003A&A...409..523R

Rouan D. 2006, 2006ISSIR...6..263R

Sahu K. 1997, 1997ASPC..119...73S

Santos N. C. 2008, 2008NewAR..52..154S

Santos N. C., Israelian G., Mayor M. 2001, 2001A&A...373.1019S

Sato B., et al. 2005, 2005ApJ...633..465S

Saumon D., Hubbard W. B., Burrows A., Guillot T., Lunine J. I., Chabrier G. 1996, 1996ApJ...460..993S

Schneider J., 2012, *the exoplanet.eu database*; [online]. Available at: <http://exoplanets.eu> [date of access: 6th of June, 2012].

Setiawan J., Henning T., Launhardt R., Müller A., Weise P., Kürster M. 2008, 2008Natur.451...38S

Sigurdsson S. 1992, 1992ApJ...399L..95S

Silvotti R., et al. 2007, 2007Natur.449..189S

Sivaramakrishnan A., Oppenheimer B. R., Hinkley S., Brenner D., Soummer R., Mey J. L., Lloyd J. P., Perrin M. D., Graham J. R., Makidon R. B., Roberts L. C., Kuhn J. R. 2007, 2007CRPhy...8..355S

Smith K. W., Bonnell I. A. 2001, 2001MNRAS.322L...1S

Soszyński I. 2006, 2006MmSAI..77..265S

Sousa S. G., Santos N. C., Mayor M., Udry S., Casagrande L., Israelian G., Pepe F., Queloz D., Monteiro M. J. P. F. G. 2008, 2008A&A...487..373S

Stevenson D. J. 1999, 1999Natur.400...32S

Strigari L. E., Barnabè; M., Marshall P. J., Blandford R. D. 2012, 2012MNRAS.423.1856S

Sumi T., et al. 2011, 2011Natur.473..349S

Sumi T. 2010, 2010ASPC..430..225S

Takeda G., Ford E. B., Sills A., Rasio F. A., Fischer D. A., Valenti J. A. 2007, 2007ApJS..168..297T

The MACHO Collaboration: D. P. Bennett, et al. 1996, 1996astro.ph.12208T

Traub W. A., Oppenheimer B. R. 2010, 2010exop.book..111T

Trilling D. E., Benz W., Guillot T., Lunine J. I., Hubbard W. B., Burrows A. 1998, 1998ApJ...500..428T

Udalski A. 2009, 2009ASPC..403..110U

Udalski A., Szymanski M. K., Soszynski I., Poleski R. 2008, 2008AcA…58…69U

Udalski A., Paczynski B., Zebrun K., Szymanski M., Kubiak M., Soszynski I., Szewczyk O., Wyrzykowski L., Pietrzynski G. 2002, 2002AcA....52....1U

Udalski A., Kubiak M., Szymanski M. 1997, 1997AcA....47..319U

Udalski A., Szymanski M., Mao S., Di Stefano R., Kaluzny J., Kubiak M., Mateo M., Krzeminski W. 1994, 1994ApJ...436L.103U

Udry S., Santos N. C. 2007, 2007ARA&A..45..397U

Veras D., Crepp J. R., Ford E. B. 2009, 2009ApJ...696.1600V

Vidal-Madjar A., Lecavelier des Etangs A., Désert J.-M., Ballester G. E., Ferlet R., Hébrard G., Mayor M. 2003, 2003Natur.422..143V

Wambsganss J. 2011, 2011Natur.473..289W

Witt H. J. 1990, 1990A&A...236..311W

Wolszczan A. 1997, 1997ASPC..119..135W

Wolszczan A. 1994, 1994Sci...264..538W

Wolszczan A., Frail D. A. 1992, 1992Natur.355..145W

Wright J. T., Upadhyay S., Marcy G. W., Fischer D. A., Ford E. B., Johnson J. A. 2009, 2009ApJ...693.1084W

Wyrzykowski Ł., Kozłowski S., Skowron J., Udalski A., Szymański M. K., Kubiak M., Pietrzyński G., Soszyński I., Szewczyk O., Ulaczyk K., Poleski R. 2011, 2011MNRAS.413..493W

Yoo J., et al. 2004, 2004ApJ...603..139Y

Youdin A. N., Shu F. H. 2002, 2002ApJ...580..494Y

Yu K. C., Bally J. 1996, 1996JGR...10114843Y

Yuan X., Cui X., Gong X., Wang D., Yao Z., Li X., Wen H., Zhang Y., Zhang R., Xu L., Zhou F., Wang L., Shang Z., Feng L. 2010, 2010SPIE.7733E..57Y

Zapatero Osorio M. R., Béjar V. J. S., Martín E. L., Rebolo R., Barradoy Navascués D., Bailer-Jones C. A. L., Mundt R. 2000, 2000Sci...290..103Z